The Surface-Forced Overturning of the North Atlantic: Estimates from Modern Era Atmospheric Reanalysis Datasets

JEREMY P. GRIST AND SIMON A. JOSEY

National Oceanography Centre, Southampton, United Kingdom

ROBERT MARSH

Ocean and Earth Science, University of Southampton, and National Oceanography Centre, Southampton, United Kingdom

YOUNG-OH KWON

Woods Hole Oceanographic Institution, Woods Hole, Massachusetts

RORY J. BINGHAM

School of Civil Engineering and Geosciences, Newcastle University, Newcastle upon Tyne, United Kingdom

ADAM T. BLAKER

National Oceanography Centre, Southampton, United Kingdom

(Manuscript received 31 January 2013, in final form 17 December 2013)

ABSTRACT

Estimates of the recent mean and time varying water mass transformation rates associated with North Atlantic surface-forced overturning are presented. The estimates are derived from heat and freshwater surface fluxes and sea surface temperature fields from six atmospheric reanalyses—the Japanese 25-yr Reanalysis (JRA), the NCEP–NCAR reanalysis (NCEP1), the NCEP–U.S. Department of Energy (DOE) reanalysis (NCEP2), the European Centre for Medium-Range Weather Forecasts (ECMWF) Interim Re-Analysis (ERA-I), the Climate Forecast System Reanalysis (CFSR), and the Modern-Era Reanalysis for Research and Applications (MERRA)—together with sea surface salinity fields from two globally gridded datasets (*World Ocean Atlas* and Met Office EN3 datasets). The resulting 12 estimates of the 1979–2007 mean surface-forced streamfunction all depict a subpolar cell, with maxima north of 45°N, near $\sigma = 27.5\,\mathrm{kg\,m^{-3}}$, and a subtropical cell between 20° and 40°N, near $\sigma = 26.1\,\mathrm{kg\,m^{-3}}$. The mean magnitude of the subpolar cell varies between 12 and 18 Sv ($1\,\mathrm{Sv} \equiv 10^6\,\mathrm{m^3\,s^{-1}}$), consistent with estimates of the overturning circulation from subsurface observations. Analysis of the thermal and haline components of the surface density fluxes indicates that large differences in the inferred low-latitude circulation are largely a result of the biases in reanalysis net heat flux fields, which range in the global mean from -13 to $19\,\mathrm{W\,m^{-2}}$. The different estimates of temporal variability in the subpolar cell are well correlated with each other. This suggests that the uncertainty associated with the choice of reanalysis product does not critically limit the ability of the method to infer the variability in the subpolar overturning. In contrast, the different estimates of subtropical variability are poorly correlated with each other, and only a subset of them captures a significant fraction of the variability in independently estimated North Atlantic Subtropical Mode Water volume.

1. Introduction

In observations as well as in ocean and climate models, a primary method for diagnosing the ocean's role in climate variability is to examine the zonally averaged meridional and vertical transport in latitude–depth coordinates. In the North Atlantic Ocean this mean meridional circulation, the Atlantic meridional overturning circulation (AMOC), is the main oceanic mechanism for the northward export of heat from the tropics. Since the deployment of the Rapid Climate Change–Meridional Overturning Circulation Heatflux

Corresponding author address: Dr. Jeremy Grist, National Oceanography Centre, European Way, Southampton SO14 3ZH, United Kingdom.
E-mail: jeremy.grist@noc.ac.uk

DOI: 10.1175/JCLI-D-13-00070.1

Array (RAPID-MOCHA) observing array at 26°N in 2004 (Cunningham et al. 2007), significant strides have been made in characterizing and understanding AMOC variability and its role in the climate system. In particular, results from the first few years of the array indicate that at that latitude the AMOC accounts for 88% of the meridional heat transport (MHT) (Johns et al. 2011). Considerable intra-annual and interannual variability has also been observed (Kanzow et al. 2007, 2010). Notably, in 2009–10 there was a temporary 30% reduction in the overturning strength relative to the mean strength measured over the first 5 years of the array (McCarthy et al. 2012).

The relationship between the AMOC in the subtropics and that in the subpolar region is a key research topic. Coupled climate models indicate that subpolar AMOC is not strongly correlated with the subtropical AMOC when it is considered in latitude–depth space (Bingham et al. 2007). A stronger connection is evident when account is taken of the different time scales associated with the southward propagation of signals through advection and coastal Kelvin waves (Getzlaff et al. 2005; Johnson and Marshall, 2002). Subpolar to subtropical coherence can also be more readily observed if instead of viewing the AMOC in level coordinates, it is examined in latitude–density space (hereinafter AMOCσ) (Zhang 2010). As well as providing a framework for understanding high- to low-latitude AMOC connections, viewing the AMOC in the latitude–density coordinates also has the advantage of being more indicative of the MHT, in the subpolar region. Furthermore it is able to distinguish circulation features associated with the formation of different water masses, such as North Atlantic Deep Water (NADW) and the North Atlantic Subtropical Mode Water (STMW), also known as Eighteen Degree Water (Zhang 2010; Grist et al. 2012).

The context of the aforementioned model-based research is that, despite altimetry and Argo float–based estimates to the south (Hobbs and Willis 2012), and monitoring of Nordic seas overflows to the north (Macrander et al. 2005; Hansen and Østerhus 2007) there is currently no model-independent observational array to characterize the subpolar AMOC, or its linkages to the subtropics. Recently Grist et al. (2012) demonstrated, using an eddy-permitting ocean-only model, that by calculating the density fluxes at the air–sea interface it is possible for the buoyancy-forced component of AMOCσ to be estimated. By using an approach that draws upon the water mass transformation concepts of Walin (1982), and additionally including the effect of Ekman transport variability, between 70% and 84% of the AMOCσ variability could be accounted for between 33° and 55°N. This followed on from earlier analyses of coupled model output in which up to 40% of the AMOC in level coordinates was accounted for using the water mass transformation-based approach (Grist et al. 2009; Josey et al. 2009).

Based on the work of Walin (1982), Speer and Tziperman (1992), and others, the method described in Grist et al. (2012) offers a way to characterize the AMOC from surface observations alone, by neglecting the effects of subsurface mixing and local changes in storage. Crucially, the utility of the surface water mass transformation method to this, and other applications, depends on the accuracy of estimates of surface air–sea fluxes over the North Atlantic. Are current estimates of surface density fluxes sufficiently accurate to allow reliable estimates of the surface water mass transformation and, ultimately, the AMOCσ? A comprehensive answer to this question would require observations of the true AMOCσ in subpolar as well as subtropical latitudes. In lieu of these, the goal of this study is to examine the range in the mean and time-varying surface-forced overturning streamfunction that result from using six state-of-the-art atmospheric reanalysis products [for estimates of net heat flux, evaporation minus precipitation ($E - P$), and sea surface temperature (SST)] and two global gridded estimates of sea surface salinity (SSS). The different reanalysis products and the different salinity products are not independent estimates; therefore, the study provides a lower bound on the uncertainty associated with current estimates of the surface-forced streamfunction. We note that Forget et al. (2011) recently calculated the STMW water mass transformation rates from two of the original atmospheric reanalysis products [the National Centers for Environmental Prediction (NCEP) and European Centre for Medium-Range Weather Forecasts (ECMWF) reanalyses]. Their study, which focused on the mean annual cycle for 1994–96, revealed large differences in estimates. In this study, a larger set of reanalysis products from the satellite era (since 1979) will be used and attention is given to both subtropical and subpolar regions; also, as well as calculating the mean transformation rate, consideration is given to recent interannual variability. By decomposing the surface density flux into its components, we reveal, in broad terms, the major cause of the spread of streamfunction estimates. This exposes the aspects of air–sea surface observations in greatest need of improvement. Finally, the ensemble mean of the time-varying streamfunction provides a description of recent ocean circulation changes that can be helpfully compared against independent time series of the water mass changes and the overturning circulation.

The structure of this paper is as follows. In section 2, the methodology behind estimating the surface-forced overturning streamfunction is described. The different

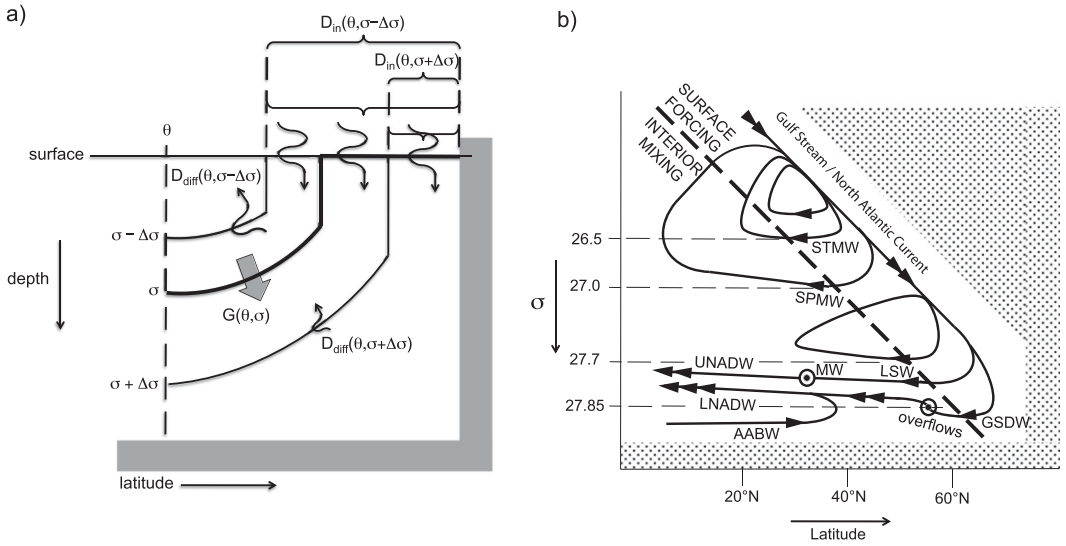

FIG. 1. (a) Schematic diagram of area integrated surface [$D_{in}(\theta, \sigma)$] and interior diapycnal [$D_{diff}(\theta, \sigma)$] density fluxes, and the net diapycnal volume flux [$G(\theta, \sigma)$] in a meridional section through an idealized North Atlantic where σ represents a zonally averaged outcropping isopycnal and θ is the latitude. (b) Schematic illustration of the relationship between the meridional overturning streamfunction in density coordinates and the formation of specific North Atlantic water masses. The thick dashed line represents the zonal maximum values of the surface density, which increases with latitude. Diapycnal volume transport at higher densities than this line is achieved by mixing processes that are diagnosed in the meridional overturning streamfunction in density coordinates but not the surface-forced overturning streamfunction. STMW and SPMW form in the subtropics and midlatitudes respectively. UNADW is a blend of LSW—some of which recirculates in the subpolar gyre—and MW. The inflection in southward transport of GSDW at around 65°N corresponds to the strong mixing processes associated with entrainment downstream of the overflows across the sills between Greenland and Scotland, which approximately doubles the transport. LNADW is thus a blend of modified GSDW and AABW.

datasets (six atmospheric reanalysis products, two global salinity products, and two independent metrics of the subpolar and subtropical Atlantic circulation) are briefly described in section 3. The mean characteristics of the surface-forced streamfunction are described in section 4 while the time-varying estimates are presented in section 5. The study's summary and conclusions are given in section 6.

2. Method

Considering the schematic meridional cross section of the North Atlantic shown in Fig. 1a and following the method previously described by Marsh (2000) and Grist et al. (2009), which was based on earlier work by Walin (1982) and Speer and Tziperman (1992), we approximate the North Atlantic as a basin closed to the north. Averaged over a region of ocean north of latitude θ, the volume flux, $G(\theta, \sigma)$ ($m^3 s^{-1}$), across an isopycnal σ, is related to the combined effects of surface density fluxes and mixing (σ is the density minus 1000 kg m^{-3}).

As has been formally shown by Nurser et al. (1999),

$$G(\theta,\sigma) = F(\theta,\sigma) - \frac{\partial D_{\text{diff}}(\theta,\sigma)}{\partial\sigma} + C(\theta,\sigma), \qquad (1)$$

where $F(\theta, \sigma)$ is the surface-forced water mass transformation rate across σ north of θ, the second term on the right-hand side is the water mass transformation due to diapycnal divergence of the diffusive density flux, $D_{diff}(\theta, \sigma)$ (kg s^{-1}), and $C(\theta, \sigma)$ is the volume flux associated with density gain from isopycnal mixing along σ, also termed cabbeling.

From Eq. (1) it can be seen that in the absence of mixing, $G(\theta, \sigma)$ can be estimated from $F(\theta, \sigma)$, that is, from surface variables alone. This diagnostic, the surface-forced overturning streamfunction, has a form similar to the zonally averaged meridional overturning in density space $\psi(\theta, \sigma)$. For example, Grist et al. (2012) show how in an ocean model $F(\theta, \sigma)$, much like $\psi(\theta, \sigma)$, features two distinct regions, corresponding to the formation of STMW and NADW. These cells are elaborated in Fig. 1b to schematically illustrate the range of water masses that are formed in surface layers and modified through mixing and entrainment processes in the interior. Surface waters advected northward in the Gulf Stream

increase in density with latitude, forming the STMW that recirculates via either the seasonal (surface influenced) or permanent (interior) thermocline. A further poleward branch along the North Atlantic Current is associated with midlatitude formation of Subpolar Mode Water (SPMW), which also recirculates via the permanent thermocline, returning to lower density in the tropics and subtropics. Farther to the north, Labrador Seawater (LSW) forms and partially recirculates in the subpolar gyre. Denser LSW escapes southward and mixes with Mediterranean Water (MW) to form the Upper NADW (UNADW) that eventually exits the North Atlantic as the lighter component of the AMOC upper branch. Last, a northernmost branch of northward flow reaches sufficiently high density to form the Greenland Sea Deep Water (GSDW) that returns south in overflows across the ridge system between Greenland and Scotland. Strong entrainment south of the ridges enhances transport and further mixing with upwelling Antarctic Bottom Water (AABW) results in the establishment of Lower NADW (LNADW), the denser component of the lower branch.

The reasons for the similarities between $F(\theta, \sigma)$, and $\psi(\theta, \sigma)$ have been detailed earlier (Marsh 2000; Grist et al. 2009) so the argument is only briefly summarized here: If it is assumed that water mass transformation in the North Atlantic is predominantly a result of surface forcing (Nurser et al. 1999), we can neglect mixing and estimate $G(\theta, \sigma)$ by calculating $F(\theta, \sigma)$. Furthermore, under the assumption of fluid incompressibility and a steady state of the water masses, all the water north of θ that is transformed across σ must be transported southward across θ. Thus by implication $F(\theta, \sigma)$ is the same as the zonally integrated meridional overturning streamfunction in density coordinates $\psi(\theta, \sigma)$. Because of the assumptions involved in this argument, and a time lag required for the southward advection of water masses, there is not exact agreement between $F(\theta, \sigma)$ and $\psi(\theta, \sigma)$. This reflects the fact that $F(\theta, \sigma)$ represents only one component of the overturning circulation, albeit the important buoyancy-forced component. The surface-forced streamfunction is, however, a legitimate measure of water mass transformation rate; and if the advective time lag is accounted for by averaging the maximum value of $F(\theta, \sigma)$ in the relevant θ–σ range, over a number of the preceding years, it can explain up to 75% of the variance in total AMOCσ in parts of the North Atlantic (Grist et al. 2012).

The value of $F(\theta, \sigma)$ is given by the following formula:

$$F(\theta, \sigma) = \frac{\partial D_{\text{in}}(\theta, \sigma)}{\partial \sigma}, \tag{2}$$

where D_{in} is the area-integrated surface density flux north of wherever the isopycnal σ outcrops (see Fig. 1a). Using the formula of Schmitt et al. (1989), we have determined D_{in} from the surface net heat and freshwater fluxes and surface temperature fields from six different atmospheric reanalysis products, and SSS from two different global gridded datasets. Values for $F(\theta, \sigma)$ were then obtained using Eq. (2) above. Because of the covariability of D_{in} and σ at the surface, $F(\theta, \sigma)$ is calculated at a monthly time scale before being averaged into annual fields.

We note that because of the lack of observations, the density fluxes specifically associated with ice melt/brine rejection are neglected. The modeling study of Grist et al. (2007) found that typically in the North Atlantic the ice-melt contribution is at least an order of magnitude smaller than that associated with heat loss, although locally it can be as important as the thermal term. Hence, neglect of this term is unlikely to have a significant impact on our results. Ice melt also impacts surface salinity and, as we utilize time-varying SSS data, the effect of ice melt/formation rate changes on surface density through anomalous freshwater advection is accounted for. The insulating effect of sea ice in reducing oceanic heat loss is also accounted for in the reanalysis estimates of net heat flux.

In examining the temporal variability of the surface-forced streamfunction, we focus on two circulation features. First, we take the maximum of the annually averaged streamfunction for the subpolar cell, specifically the maximum value of $F(\theta, \sigma)$ north of 45°N, to be a measure of the annual surface-forced overturning circulation at 45°N or the subpolar/NADW transformation rate. Second, we take the maximum of the annually averaged streamfunction for the subtropical cell, that is between 20° and 40°N and where σ is between 25.175 and 26.375 kg m^{-3}, to be indicative of the subtropical overturning or transformation rate. We note that these measures of the circulation, although referred to as overturning in density space, incorporate horizontal gyres in level coordinates. For example, in the lighter subtropical cell some of the warm, lighter waters flowing northward in the Gulf Stream recirculate as cooler, denser waters farther east in the gyre interior.

3. Datasets

a. *Atmospheric reanalyses*

The main datasets used are six atmospheric reanalysis products that span 1979–2011, a period that has been referred to as the "Modern Era" (Table 1). The products involve the assimilation of historical, quality-controlled atmospheric and surface data into the numerical weather prediction (NWP) model of a particular organization.

TABLE 1. Summary of atmospheric reanalysis products used to provide net heat flux, $E - P$, and SST for this study.

Dataset	Abbreviation	Prescribed SST field	Time span	Approximate horizontal resolution	Reference
Japanese 25-yr Reanalysis (JRA-25)–Japanese Meteorological Agency (JMA) Climate Data Assimilation System	JRA	Ishii et al. (2005)	1979–2007	1.125° × 1.125°	Onogi et al. (2007)
NCEP–NCAR reanalysis	NCEP1	Reynolds and Smith (1994)	1979–2010	1.875° × 1.915°	Kalnay et al. (1996)
NCEP–DOE reanalysis II	NCEP2	Taylor et al. (2000)	1979–2011	1.875° × 1.915°	Kanamitsu et al. (2002)
ECMWF Interim Re-Analysis	ERA-I	Before 2002: Fiorino (2004); 2002 onward: the operational forecast system (see Dee et al. 2011)	1979–2011	1.500° × 1.500°	Dee et al. (2011)
NCEP Climate Forecast System Reanalysis	CFSR	Coupled ocean–atmos. reanalysis	1979–2009	0.500° × 0.500°	Saha et al. (2010)
National Aeronautics and Space Administration (NASA) Modern-Era Reanalysis for Research and Applications	MERRA	Reynolds et al. (2002)	1979–2011	0.667° × 0.500°	Rienecker et al. (2011)

The exception to this is the Climate Forecast System Reanalysis (CFSR), which is a coupled ocean–atmosphere reanalysis and therefore involves the assimilation of ocean and atmosphere data into their respective models, which are linked in a physically consistent manner. Throughout the approximately 30-yr period covered, the assimilation schemes and atmospheric or ocean model stay constant, but the number of available observations vary. The availability of reanalysis fields for recent years varies slightly and therefore in this study they have slightly different lengths. The period common to all the datasets is 1979–2007. It is this period that is used to calculate means and departure from means. The specific fields used to calculate the surface density flux are surface evaporation minus precipitation ($\mathrm{m\,s^{-1}}$), net surface heat flux (the sum of latent, sensible, net shortwave radiation, and net longwave radiation fluxes; $\mathrm{W\,m^{-2}}$), and SST (°C). We note that precipitation is a model output not itself constrained by precipitation data, but rather by the other assimilated observations and the physics and dynamics of the model. We also note that the SST fields are entirely based on observations. The SST fields are important inputs to the NWP model but are not dependent on it. The different sources of SST fields for the reanalyses are detailed in Table 1. Again, the exception is the ocean–atmosphere reanalysis CFSR, in which SSTs are assimilated into the ocean component of the coupled ocean–atmosphere model. All the variables, regardless of the extent to which they are constrained by observations, form part of the internally consistent reanalysis product. A summary of the reanalysis products is included in Table 1. Further details are included in the relevant listed references.

b. Sea surface salinity data

To calculate the surface density fluxes, SSS is taken from the surface level of the *World Ocean Atlas* (*WOA*) *2009* (*WOA09*; Antonov et al. 2010) and Met Office EN3, version 2a (Ingleby and Huddleston 2007), global gridded products. These widely used datasets have different quality control and objective analysis procedures, but share the main sources of surface and subsurface data (e.g., World Ocean Database, Global Temperature and Salinity Profile Program, and Argo Float Profiles). Both *WOA* and EN3 have 1° × 1° horizontal resolution. The temporal resolution of *WOA* is annual; however, prior to 2005 the annual fields are in fact pentadal averages (e.g., 1977–81 for 1979). As $F(\theta, \sigma)$ is originally calculated at each monthly time step (section 2), the same annual *WOA* SSS fields were used for each of the 12 months of the corresponding year. Although the EN3 data are available in monthly format for the entire study period, monthly data were averaged into annual fields and used in the same manner as *WOA* to allow a direct comparison of the results using the two salinity datasets and avoid potential differences arising from the treatment of the seasonal cycle.

c. Sea level data

A sea level time series that has been proposed as a proxy for the subpolar overturning (Bingham and Hughes 2009, hereafter BH09), is compared with the

temporal variability of the subpolar circulation calculated in this study. The time series, updated from BH09, is based on a composite of 10 tide gauge records on the U.S. East Coast between 40°N (New York) and 45°N (Yarmouth) spanning the period 1948–2012. These records were obtained from the Permanent Service for Mean Sea Level (PSMSL; Woodworth and Player 2003; http://www.psmsl.org/data/obtaining/). We use only revised local reference (RLR) data, which are given as monthly mean values. The sea level records are corrected for the inverted barometer (IB) response of the sea surface to atmospheric pressure variations using NCEP monthly sea level pressure interpolated to the tide gauge positions. Before forming the composite time series, the trend and mean seasonal cycle are removed from each IB corrected tide gauge record and a 13-month running mean filter is applied to remove remaining intra-annual variability. Based on the reasoning given by BH09, the sign of the composite sea level record is reversed to give an indication of the temporal changes in the AMOC between 40° and 45°N.

d. *STMW volume time series*

Time series of STMW volume from Kwon and Riser (2004; hereafter KR04) is extended for the recent 10 years, so that the time series spans 50 years from 1961 to 2010. STMW volume is calculated independently for each season (i.e., February–April, May–July, etc.) from the objectively mapped temperature field based on the temperature profiles from the *WOA01* for 1961–2000 (KR04), and *WOA09* and its online updates for 2001–10. The STMW is identified as a thermostad ($dT/dz \leq 0.006°C\,m^{-1}$) between 17° and 19°C (see KR04 for details).

4. Mean surface-forced overturning 1979–2007

In this section, we first examine the range of estimates in the mean surface-forced overturning that arise from using six reanalysis products and two surface salinity products. These estimates are placed in the context of previous work. Following this, where the range of estimates is particularly large, we investigate potential causes of these differences.

a. *Reanalysis-based estimates of the mean surface-forced streamfunction*

The mean surface-forced overturning streamfunctions for the period 1979–2007 calculated from the six reanalysis products and SSS from *WOA* are plotted in Fig. 2. We note the mean values of $F(\theta, \sigma)$ derived using SSS from the EN3 dataset are very close but not exactly the same; since they are visually hard to distinguish from the *WOA* derived streamfunctions, they are not shown. For a more helpful comparison of the *WOA* and EN3 derived streamfunctions, the maximum value of $F(\theta, \sigma)$ for each density bin, for all 12 estimates, is plotted in Fig. 3a. Common features of the streamfunctions in Fig. 2 (also shown schematically in Fig. 1b) include a large positive (clockwise) cell that spans at least the density range 25.8–28.0 $kg\,m^{-3}$ and from the equator to 70°N. Within this cell, which depicts northward bound water becoming denser and returning south at greater densities, there are two distinct maxima. First, the cell centered near $\sigma = 27.5\,kg\,m^{-3}$ is associated with the overturning in the subpolar region. The convergence of streamlines at densities greater than this maximum is associated with the formation of NADW. Second, the cell with maxima near $\sigma = 26.1\,kg\,m^{-3}$ is associated with subtropical recirculation and the convergence of streamlines at densities greater than the maxima (i.e., $26.2 < \sigma < 27.0\,kg\,m^{-3}$) is associated with STMW formation. These features are also prominent in state estimated or modeled $\psi(\theta, \sigma)$ (see Fig. 7 in Hakkinen et al. 2011; Fig. 1a in Zhang 2010; Fig. 4b in Grist et al. 2012). In those depictions, streamlines (denoting deep dense water moving to a lighter density class) close in the tropics and subtropics where seasonal mixed layer entrainment plays an important role in water mass transformation (Nurser et al. 1999). With mixing neglected, the streamlines of $F(\theta, \sigma)$ do not close in this way. We will first consider the spread of estimates in the mean NADW transformation rate, and then turn our attention to the subtropics, finally considering other features of the inferred surface-forced circulation, such as the counter clockwise cells in the tropics and subtropics.

1) SUBPOLAR CELL

The reanalysis-based estimates of transformation rates in the θ–σ space associated with subpolar overturning range from 12 Sv (CFSR with EN3) to 18 Sv [the NCEP–National Center for Atmospheric Research (NCAR) reanalysis (NCEP1) with *WOA*] (Fig. 3a; $1\,Sv \equiv 10^6\,m^3\,s^{-1}$). To put this in context, the AMOCσ estimates of six occupations of the Greenland (60°N) to Portugal (40°N) Observatoire de la Variabilité Interannuelle à Decennale (OVIDE) line range from 12.2 to 18.5 Sv between 1997 and 2010 (Lherminier et al. 2007, 2010; Gourcuff et al. 2011). However, although surface flux and hydrographic estimates are in relative agreement we note that they do not represent identical features of the subpolar overturning. In particular, before crossing the OVIDE line downstream, NADW formed by surface fluxes undergoes modification from both mixing and entrainment. Mixing may act to reduce the amount of surface-forced NADW transported south of the OVIDE

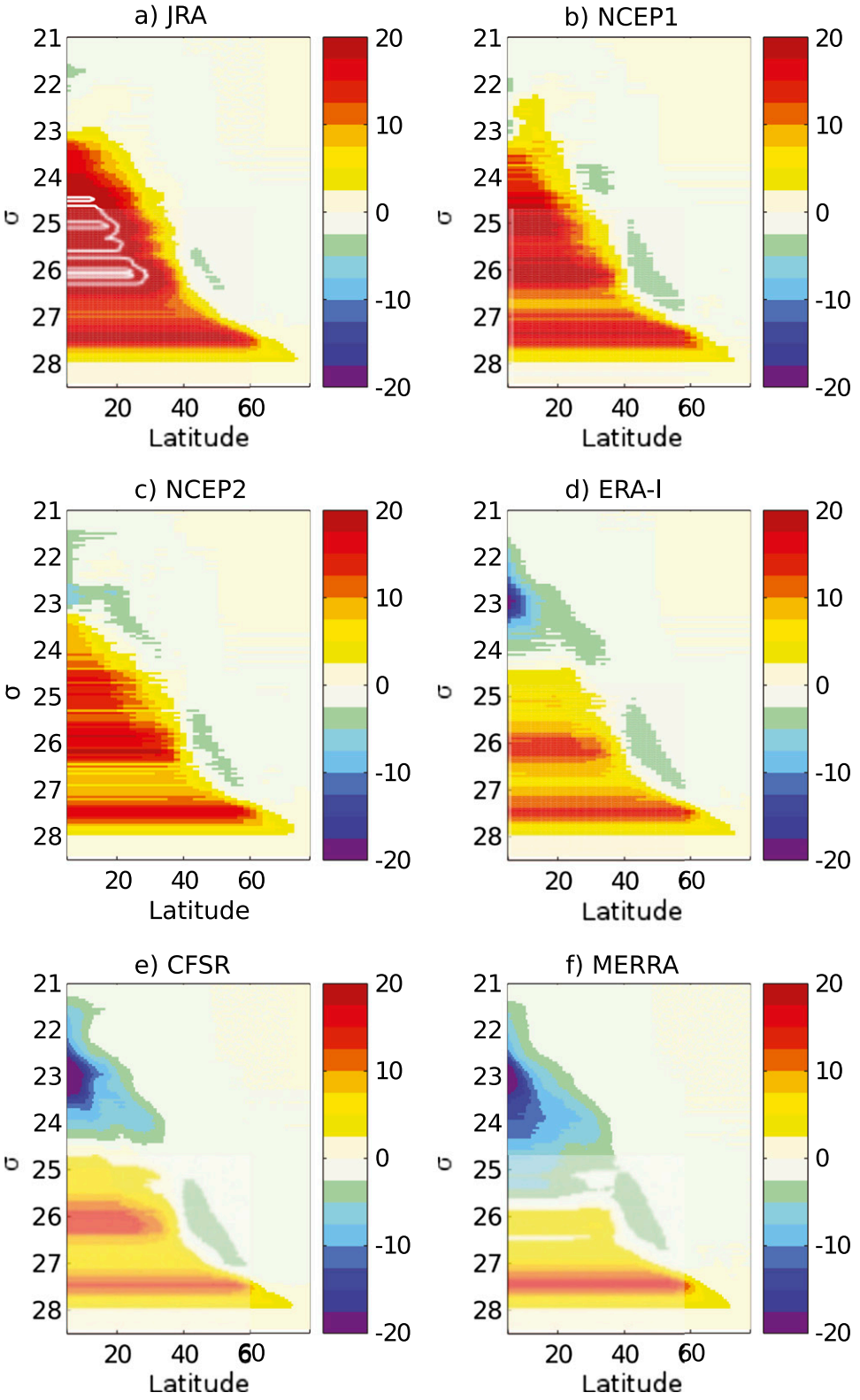

FIG. 2. Mean surface-forced streamfunction (Sv) (1979–2007) for the North Atlantic Ocean using surface salinity from *WOA* and surface fluxes and SST fields from (a) JRA, (b) NCEP1, (c) NCEP2, (d) ERA-I, (e) CFSR, and (f) MERRA. The white contours in (a) are additional contours for 24 and 28 Sv.

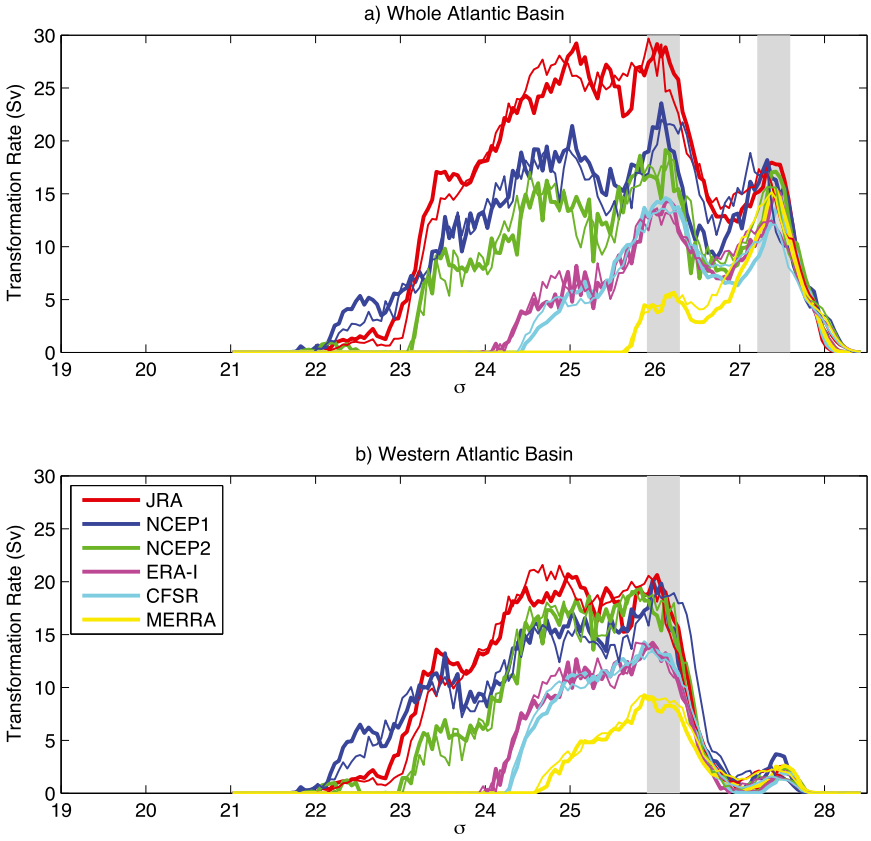

FIG. 3. (a) Maximum transformation rate (Sv) for each density bin from the mean surface-forced streamfunction for the North Atlantic Ocean, 1979–2007. The thick lines indicate estimates calculated with *WOA* SSS and the thin lines indicate estimates calculated with EN3 SSS. The atmospheric reanalysis used for SST and the surface fluxes are indicated in the legend. (b) As in (a), but calculated from the surfaced forced streamfunction of the western (west of 40°W) half of the Atlantic only. The vertical gray bars denote the location of the subtropical and subpolar maxima in transformation rates near $\sigma = 26.1\,\mathrm{kg\,m^{-3}}$ and near $\sigma = 27.5\,\mathrm{kg\,m^{-3}}$, respectively.

line, although it has been argued (Nurser et al. 1999) that its influence in this region is relatively small. Furthermore, mixing could alter the density structure without changing the value of the maximum overturning. However, the process of entrainment is expected to significantly increase NADW formed north of the Greenland–Scotland Ridge, as it overflows from the sills and is transported southward (Dickson and Brown 1994), with hydrographic observations indicating a doubling of transport (Hansen and Østerhus 2000). A further limitation of the comparison is due to the fact that the OVIDE line is upstream of any surface-forced formation of Labrador Seawater.

2) SUBTROPICAL CELL

Turning to the subtropics, all depictions of the streamfunction (Fig. 2) show a maximum in the transformation rate near $\sigma = 26.1\,\mathrm{kg\,m^{-3}}$ between 20° and 40°N, ranging from 6 Sv (MERRA) to 29 Sv (JRA) (Fig. 3a). Using the Isemer and Hasse (1987) air–sea flux dataset, Speer and Tziperman (1992) found a maximum transformation rate of about 30 Sv in the same density range. Lumpkin and Speer (2003) used observations from hydrographic sections and current meters, along with surface fluxes of da Silva et al. (1994), in an inverse model to calculate a maximum subtropical transformation rate of 19.2 ± 3.3 Sv. It is notable that our 12 estimates of transformation rates yield a much larger range, and thus greater uncertainty, in the subtropics than in the subpolar region. The causes of this larger range in the subtropics will be considered in section 4b. However, we will first consider the implications of the large range in subtropical transformation rates for estimates of the formation rate of STMW.

The accumulation, or formation of water mass, between two isopycnals σ and $\sigma + d\sigma$ is determined by the convergence in transformation rate, that is,

TABLE 2. Tables showing the maximum of the mean annual subtropical transformation rate (Sv) and the mean annual STMW formation rate from the 12 reanalysis-based estimates of the surface-forced overturning streamfunction (for the whole Atlantic basin). Normal and italic text denote the use of *WOA* and EN3 SSS, respectively. Also shown are the global mean oceanic heat fluxes ($W\,m^{-2}$) for 1979–2007 for the different atmospheric reanalysis products. Positive indicates oceanic heat gain.

	JRA	NCEP1	NCEP2	ERA-I	CFSR	MERRA
Maximum of mean annual subtropical transformation rate (Sv)	29.1	23.6	19.1	14.3	14.6	5.7
Subtropical transformation rate (Sv)	*29.1*	*22.0*	*18.3*	*13.6*	*13.6*	*5.6*
Mean annual STMW	14.0	5.9	6.9	5.0	7.7	−1.4
Formation rate (Sv)	*8.5*	*5.9*	*8.9*	*2.1*	*4.6*	*−4.1*
Global mean heat flux ($W\,m^{-2}$)	−12.5	+3.7	+4.3	+10.5	+12.9	+18.5

$$M(\sigma) = -[F(\sigma + d\sigma) - F(\sigma)], \tag{3}$$

where $M(\sigma)$ is the *formation rate* in Sverdrups (Forget et al. 2011). Using density limits of STMW, σ and $\sigma + d\sigma$ defined as 26.2 and 27.0 $kg\,m^{-3}$ as in Speer and Tziperman (1992), the 12 reanalysis-based estimates of transformation rate were used to calculate the STMW formation rate. The resulting range of estimates is between −4 and 14 Sv. Interestingly, both of the estimates made with the MERRA dataset yield negative values of $M(\sigma)$, implying no net STMW formation. The discrepancy of this result with previous work on STMW formation (e.g., KR04) suggests that the mean MERRA fluxes are not accurate in this region. For the other datasets, the formation rate is between 2 and 14 Sv (see Table 2). In context, the earlier flux-based estimates of Speer and Tziperman (1992) are toward the upper end (12.8 Sv) of this range, while recent estimates with a version of NCEP fluxes constrained by ocean data (Forget et al. 2011) are toward the lower end (4.6 Sv) of this range. An estimate independent of air–sea fluxes, but based on hydrographic observations of the difference between STMW volume in the autumn and spring, corresponds to a mean annual formation rate between 3 and 4 Sv (KR04).

Some of the differences between the reanalysis and hydrography-based estimates of STMW formation rate may reflect the fact that in Fig. 2 we are depicting the circulation, zonally averaged over the width of the Atlantic, whereas the KR04 estimates are confined to the western half of the basin. However, if the calculation in Fig. 2 is restricted to the western half of the basin, as shown in Fig. 3b, then although the range in maximum subtropical transformation rate (8–21 Sv) and the STMW formation rate (7.5–17.5 Sv) is considerably smaller, the magnitude of STMW formation rate is high relative to KR04.

We note two possible reasons for the tendency of surface fluxes to overestimate STMW relative to that from the KR04 calculations from in situ observations. First, the flux-based estimates neglect other processes that act to retard STMW formation. These processes include the net effect of seasonal mixed layer entrainment (Nurser et al. 1999) and lateral fluxes, probably associated with Gulf Stream meandering, which act to slow the deepening of the mixed layer and the subsequent STMW formation (Davis et al. 2013). Second, the KR04 estimate could be an underestimation since the seasonal resolution of their time series does not fully resolve the difference between the maximum and minimum volume (e.g., Forget et al. 2011; Davis et al. 2013). Shorter time series of monthly resolution indicate that the seasonal resolution in KR04 may underestimate the annual production of STMW by as much as a factor of 2 (Kwon 2003; Forget et al. 2011). Considering recycling of the portion of newly formed STMW within the surface mixed layer due to the rapid restratification, the season-mean-based estimate could be close to the subduction rate at the bottom of the deepest winter mixed layer, while the monthly-mean-based estimate may be more comparable to the surface flux–based formation rate. Given the difficulty in quantifying these effects, it is clear that reconciliation of STMW formation rate estimates from state-of-the-art, unconstrained reanalysis fluxes with estimates of STMW volume change remains a challenging area of research (e.g., Joyce 2012; Forget et al. 2011).

3) OTHER CIRCULATION FEATURES

Four of the six streamfunctions—JRA, NCEP1, NCEP2, and ERA-I—show a secondary subtropical maximum just south of 20°N near $\sigma = 25.1\,kg\,m^{-3}$ (Fig. 2), although this feature is very weak in ERA-I. This circulation feature is associated with a weak maximum in the density flux gain just to the south of the 25.1 $kg\,m^{-3}$ isopycnal (light gray contour Fig. 4). This secondary maximum in subtropical surface-forced overturning is sometimes evident in model depictions of AMOCσ as a weak maximum in the lightest, most southern part of the subtropical overturning cell (e.g., Fig. 1a in Zhang 2010; Fig. 3b in Grist et al. 2012). The three reanalysis-based $F(\theta, \sigma)$ estimates that have poorly resolved or nonexistent

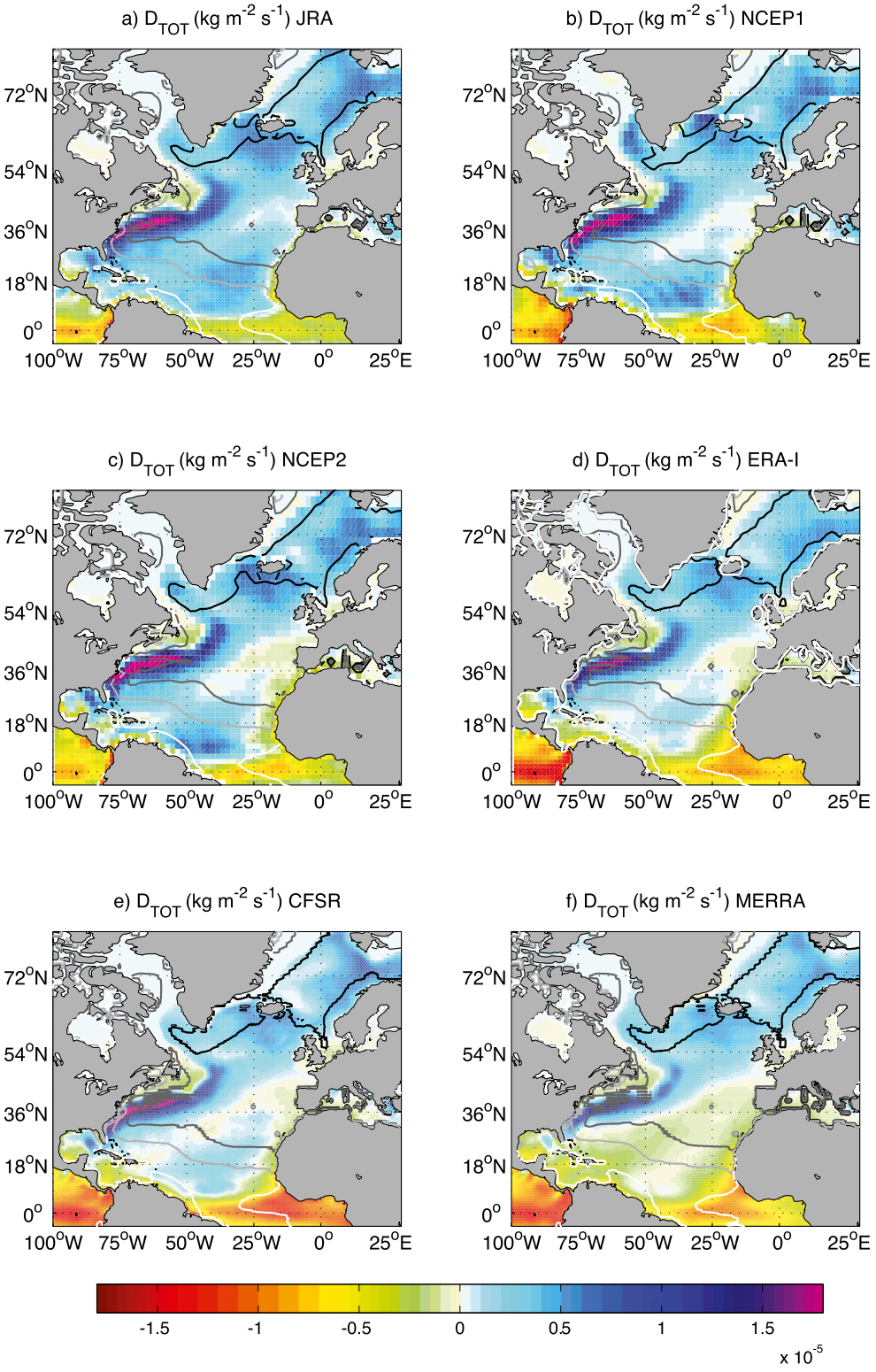

FIG. 4. Mean March surface density flux (kg m^{-2} s^{-1}) for 1979–2007 calculated with *WOA* SSS and surface fluxes and SST from six different atmospheric reanalysis products: (a) JRA, (b) NCEP1, (c) NCEP2, (d) ERA-I, (e) CFSR, and (f) MERRA. The contours denote relevant March surface isopycnals: 27.5 (black), 26.1 (dark gray), 25.1 (light gray), and 23.1 kg m^{-3} (white). Positive values denote ocean surface density gain.

secondary subtropical maxima (MERRA, ERA-I, and CFSR) all have a strong anticlockwise cell at low latitudes. This cell, which is centered on the equator but extends as far north as 40°N in the case of MERRA, represents a lightening of the already light surface waters by a negative density flux to the south of the relevant isopycnal (as examples, the cases of $\sigma = 23.1$ and $25.1\,\mathrm{kg\,m^{-3}}$ are shown in Fig. 4). The degree to which this cell (not seen in model AMOCσ) extends northward (and toward denser waters) is to a large extent determined by the location of the zero line of the surface density flux. This line lies to the north (between 35° and 55°N) in MERRA and CFSR (Figs. 4e,f) but at the other extreme between 10° and 15°N in JRA (Fig. 4a). The relative importance of the thermal and haline terms to determining the magnitude of the density fluxes, and therefore the location of the zero line, is considered in the next section.

Another feature common to a greater or lesser extent to all versions of $F(\theta, \sigma)$ but typically absent in $\psi(\theta, \sigma)$ is the weak anticlockwise cell, centered near $\sigma = 26.2\,\mathrm{kg\,m^{-3}}$, between 40° and 60°N, depicting increasing density in relatively dense waters and decreasing density of relatively light waters. This cell is not present in modeled or ocean state estimated versions of $\psi(\theta, \sigma)$ (Hakkinen et al. 2011; Grist et al. 2012), possibly due to the opposing effect of seasonal mixed layer entrainment making dense water lighter and light waters more dense.

A comparison of the maximum transformation rates in Fig. 3 confirms our previously stated result: the selection of salinity product (*WOA* or EN3) makes little difference to the transformation rates compared to the range of values possible when changing the reanalysis product. This is not likely to be indicative of a high degree of accuracy in the two salinity fields; rather, it implies a largely common pool of source data for the two products. In the tropics and subtropics there is considerable diversity in the inferred mean ocean circulation, with some reanalysis-based estimates yielding strong anticlockwise low-latitude circulations (Figs. 2 and 3). Again, the primary cause of this spread in results appears to be differences in the surface fluxes as opposed to the SSS fields.

b. *Causes of differences in the subtropical cell*

In this section we explore the cause of the large spread in estimates of subtropical transformation rates in Fig. 3. We note that surface water mass transformation rates are equivalent to the diapycnal divergence of the area-integrated surface density flux in the vicinity of the relevant outcropping isopycnal [Eq. (2)]. Figure 4 shows the mean density flux and selected surface isopycnals for March, the month of strongest surface density gain. Differences in the peak subtropical transformation rate will be caused in particular by differences in density flux to the south of the in $\sigma = 26.1\,\mathrm{kg\,m^{-3}}$ isopycnal. An examination of the six density flux fields with *WOA* SSS (Fig. 4) suggests that the main differences in $\sigma = 26.1\,\mathrm{kg\,m^{-3}}$ density fluxes are of the magnitude of Gulf Stream fluxes and the sign of the fluxes in the eastern half of the basin. For example, considering the density flux fields for the greatest (JRA) and weakest (MERRA) transformation rate, the peak density fluxes to the south of the $26.1\,\mathrm{kg\,m^{-3}}$ isopycnal (dark gray line) in the Gulf Stream region are stronger in JRA ($1.5 \times 10^{-5}\,\mathrm{kg\,m^{-2}\,s^{-1}}$) than in MERRA ($0.9 \times 10^{-5}\,\mathrm{kg\,m^{-2}\,s^{-1}}$). In addition, along the $26.1\,\mathrm{kg\,m^{-3}}$ isopycnal, east of 50°W the MERRA density flux is negative (density loss) whereas the JRA density flux is positive for the whole breadth of the basin. Thus, the large spread in subtropical transformation rates from atmospheric reanalysis appears to be associated with 1) different strengths of Gulf Stream density flux and 2) different locations in which the density flux transitions from positive to negative.

To understand the causes of the different mean density fluxes that lead to the diverse depictions of the surface-forced streamfunction, we decompose the annual mean surface density flux into their two component parts, the haline component (Fig. 5) associated with $E - P$ and the thermal component (Fig. 6) associated with the net heat flux. It is evident that the haline density flux is the much smaller contributor to the total density flux. This result for the North Atlantic has been noted in observations (Schmitt et al. 1989; Howe and Czaja 2009) and coupled climate models (Grist et al. 2007; Langehaug et al. 2012). The regions where the haline flux is strongest, and makes the greatest contribution to the overall density flux, are the strong evaporative zone in the eastern subtropics and the region of large negative density flux associated with precipitation in the intertropical convergence zone. Both of these areas are away from main regions of surface water mass transformation. We also note that there is relatively little difference in the haline density flux fields from the six reanalysis products. In contrast, the thermal density flux (Fig. 6) accounts for the majority of the total density flux, particularly in the region of water mass formation (the Gulf Stream, the Subpolar Gyre, and the Nordic seas) and there are considerable differences between the different reanalysis-based estimates.

While the thermal density flux fields share broadly similar spatial structure, there are substantial differences in magnitude and the location of transition from positive to negative values. The transition zone between

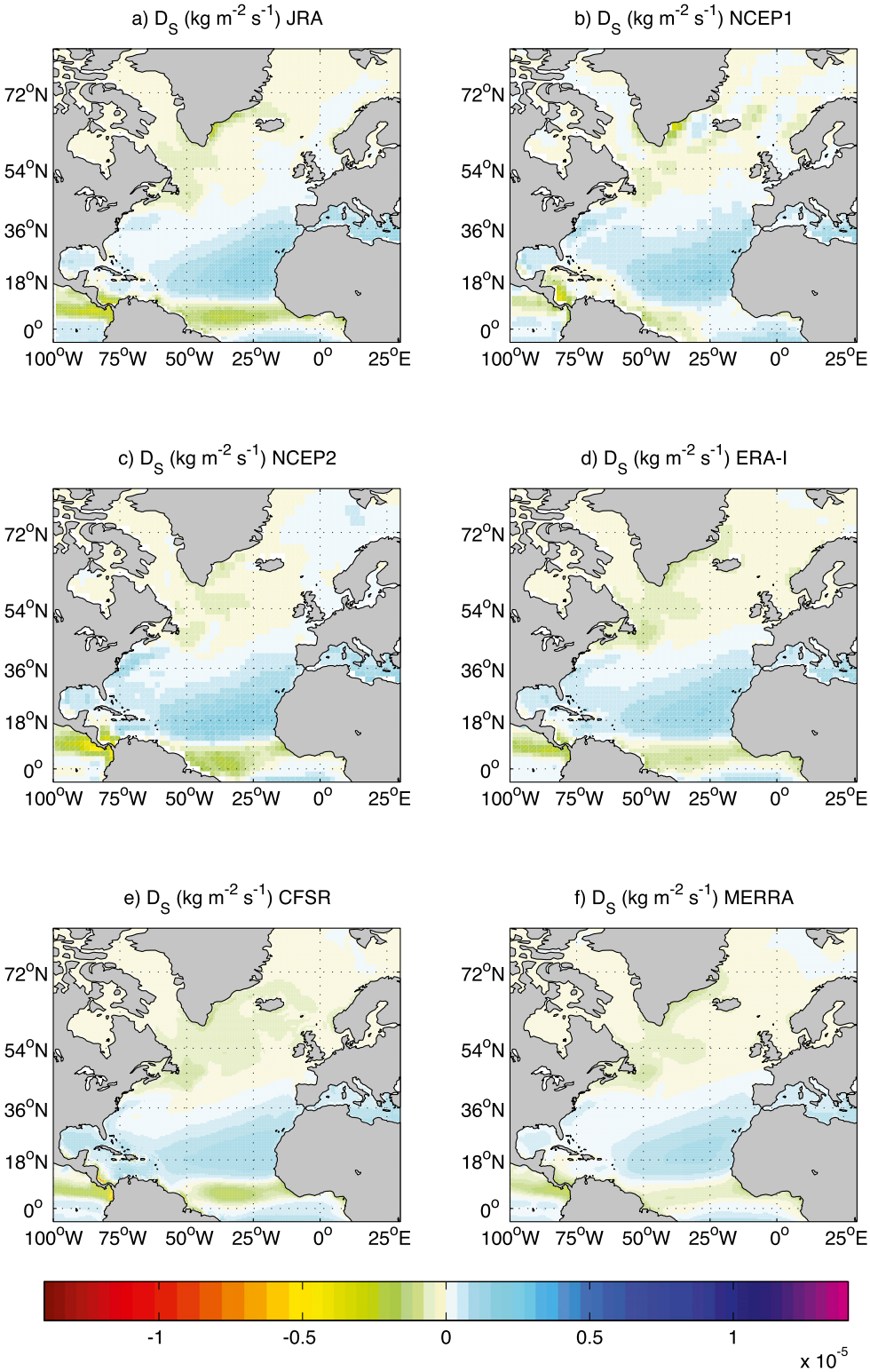

FIG. 5. Mean annual haline density flux, 1979–2007 (kg m^{-2} s^{-1}), for the North Atlantic Ocean using surface salinity from *WOA* and surface fluxes and SST fields from (a) JRA, (b) NCEP1, (c) NCEP2, (d) ERA-I, (e) CFSR, and (f) MERRA.

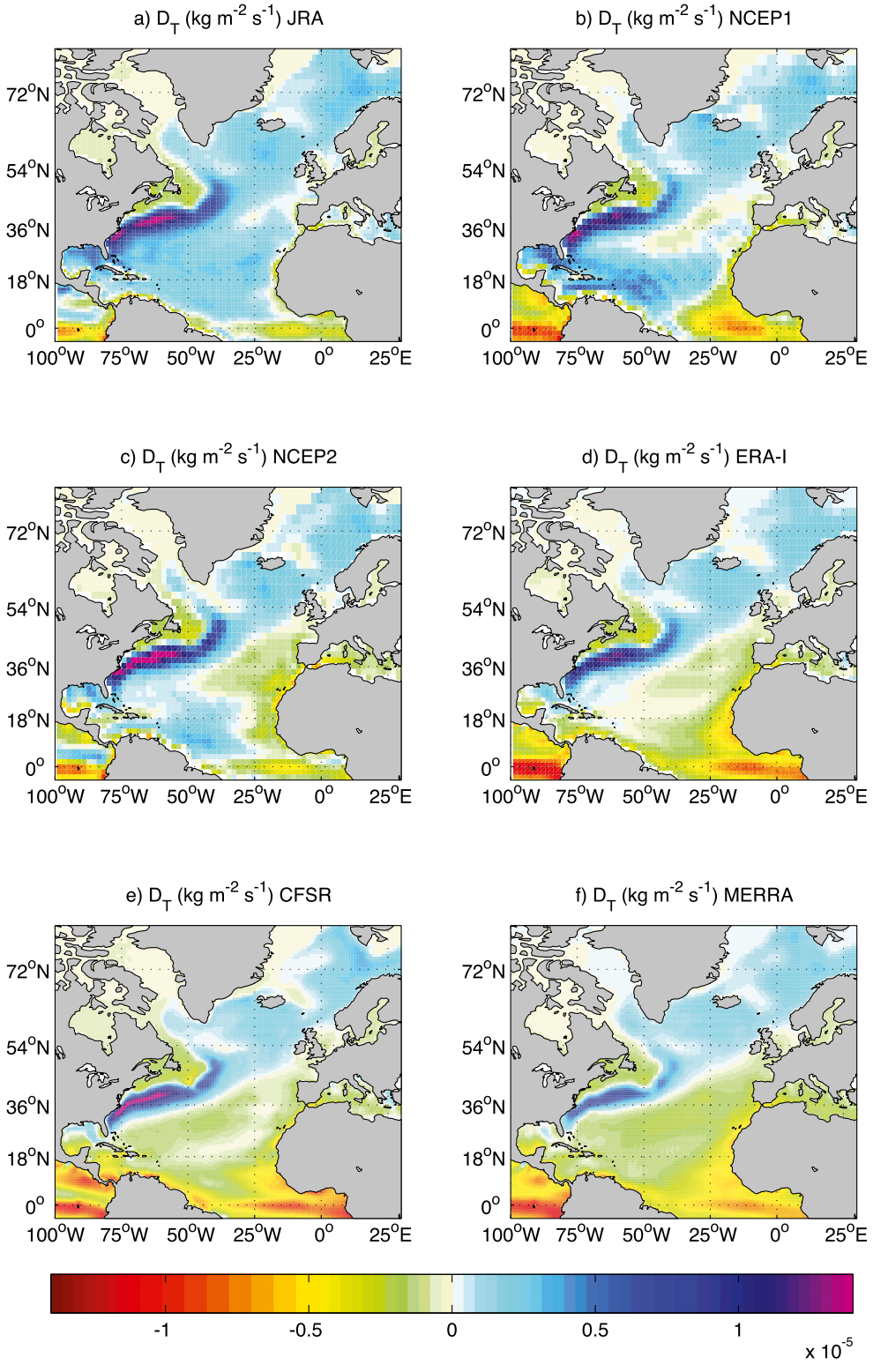

FIG. 6. As in Fig. 5, but for mean annual thermal density flux.

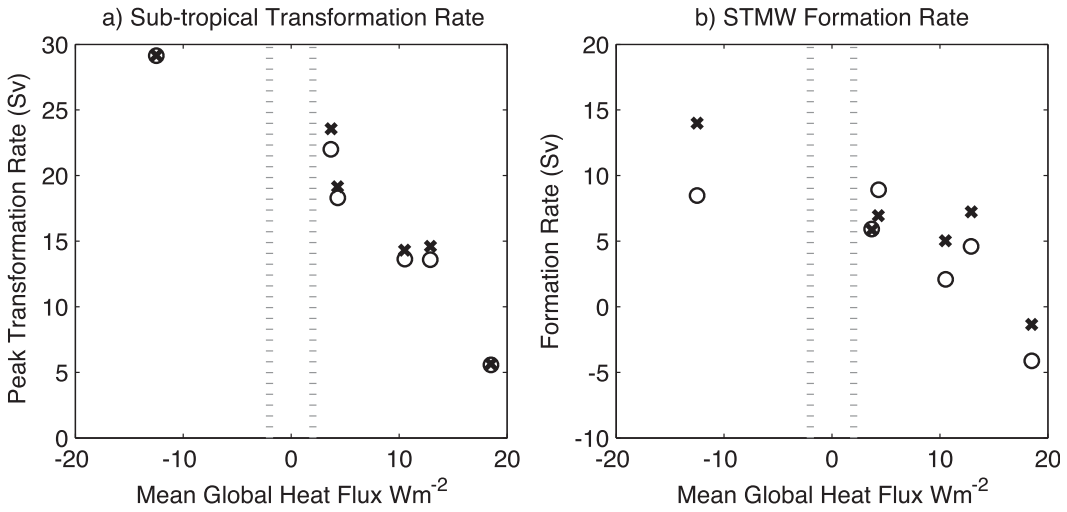

FIG. 7. Scatterplots showing 12 estimates of (a) the maximum of the mean subtropical transformation rate (Sv) ($26.0 < \sigma < 26.2\,\mathrm{kg\,m^{-3}}$) and (b) the maximum of the mean STMW formation rate (Sv), both against the mean global ocean heat flux ($\mathrm{W\,m^{-2}}$) of each of the reanalysis sets used. The vertical dotted lines denote the global ocean heat budget range from -2 to $2\,\mathrm{W\,m^{-2}}$.

low-latitude heat gain (negative density flux) and high-latitude heat loss (positive density flux) varies from a line linking 30°N on the eastern U.S. coast to the British Isles (54°N) in MERRA, to a couple of degrees north of the equator in JRA. This variation, which also largely determines the zero line of the total density flux discussed earlier, reflects the imbalances in the global ocean heat budget in each of the reanalysis products. That is to say, the greater the positive heat flux bias, the more northerly the transition from (thermal and total) density flux loss to gain. The majority of the reanalysis products have global heat budgets with considerable (i.e., $>10\,\mathrm{W\,m^{-2}}$) imbalances (see Table 2). The only products that approach heat budget closure for the study period are NCEP1 ($+3.7\,\mathrm{W\,m^{-2}}$) and NCEP2 ($+4.3\,\mathrm{W\,m^{-2}}$).

A further implication of this analysis is that in θ–σ regions, where reanalysis products display a strong connection between global ocean heat flux and local density flux, much of the spread in subtropical transformation rates may reflect the different biases in global ocean budgets. This point is illustrated in Fig. 7a, which shows a clear inverse relationship between the global ocean heat budget and the maximum transformation rate in the subtropics. There is a similar (although not quite as strong) relationship between the STMW formation rate estimated from a reanalysis product and the global heat budget of the reanalysis, as shown in Fig. 7b. The vertical dotted lines in Fig. 7 denote the range from -2 to $2\,\mathrm{W\,m^{-2}}$ in the global ocean heat budget. Grist and Josey (2003) argue that this range is a suitable physical constraint on the Global Ocean heat budget, taking into account observed changes in ocean temperature. Interpolation between these limits therefore may also indicate the range of more physically realistic values for the annual transformation and formation rates.

In summary, in this section it has been shown that Walin-type estimates of the mean subpolar transformation rate are only moderately sensitive to the choice of atmospheric reanalysis and fall within the range of recent hydrographic estimates of the subpolar AMOCσ strength. In contrast, flux-based estimates of subtropical transformation and STMW formation rates range widely and, even when confined to the western basin, generally lie outside the range estimated by observed STMW volume changes. The greater spread in estimated transformation rates in the subtropics is indicative of the large spread in density fluxes in the region. The large spread in density flux estimates is predominantly due to differences in the surface heat fluxes as opposed to differences in the salinity fields or the freshwater fluxes. Finally, the differences in the air–sea heat fluxes to a large extent reflect their mean global ocean heat budgets.

5. Recent temporal variability in the surface-forced streamfunction

a. *Subpolar circulation*

In previous work we have examined the relationship between variability in the subpolar or NADW transformation rate inferred from the Walin framework and the AMOC itself. In a range of coupled models it was found that increases in AMOC strength lagged increases

in surface-forced subpolar transformation rate by 3–5 years (Grist et al. 2009). It was also found that this transformation rate can be used to explain the greatest amount of AMOC variability by calculating its 10-yr past average (Josey et al. 2009; Grist et al. 2009; Grist et al. 2012). Note that by ''10-yr past average'' we refer to the average of the current year and the nine previous years. In this section, we examine the range of reanalysis-based estimates of recent variability using the 10-yr past average of the NADW transformation rate. Before doing this we will examine the spread of results in the unaveraged time series, because the NADW transformation rate is also an important index of the variability in the North Atlantic subpolar circulation.

The time-varying anomalies of the subpolar transformation rate (as defined in section 2) with respect to the 1979–2007 mean for the 12 different estimates are shown in Fig. 8a. There is considerable agreement between the different estimates; the mean correlation r between the estimates is 0.71 and the range is between 0.48 and 0.90. The standard deviation of each time series ranges between 2.5 and 3.4 Sv. The ensemble means of annual anomalies for both SSS products are plotted in Fig. 8b with the standard deviations of the ensembles as error bars. The mean estimates fall within the combined error range in all years except 1986, 1989, 2006, and 2010, implying that the choice of salinity product does not greatly affect the temporal variability. The two mean time series depict cyclic variability of amplitude around ± 5 Sv on a time scale on the order of 5 years, superimposed on a weak decline from 1979 to 2005.

Based on the strength of geostrophic balance for large-scale flows, Bingham and Hughes (2008) show that the zonal integral of the meridional transport is determined by the difference between the bottom pressure anomalies at the easternmost and westernmost points of the ocean floor at a given depth. They further argue that as most of the variability in this pressure difference is in the west, and that the variability is primarily on the shelf, boundary bottom pressure can be estimated by sea level anomalies. Sea level records from the eastern U.S. seaboard may thus provide an indicator of the long-term evolution of AMOC strength (BH09). The Walin method attempts to capture the light to dense transformation of water from density fluxes at the air–sea interface, while assuming coherence between the upper and lower AMOC branches, and the BH09 analysis captures the signal of the passage of this dense water mass along the deep western boundary. Similarities might therefore be expected in the respective time series although, unlike the Walin approach, the BH09 time series also reflects variability in the wind-forced component of the AMOC.

The BH09 time series (Fig. 8b) does have similarities with transformation estimates from this study (coincident maxima in 1990, 1995, and 2008 and minima in 1987, 1992, 1997, and 2005), but it is not significantly correlated over the full length of the time series. The lack of a significant correlation may be due a combination of the assumptions in both approaches and the additional wind-forced variability captured in BH09, and it may also reflect the extent to which a scarcity of surface air and humidity observations limits estimates of mid- to high-latitude air–sea heat flux variability. These issues, and the relationship between the BH09 and Walin signal, warrant further investigation. However, the extent to which these independent approaches to estimate AMOC variability share similarities suggest that they may together provide useful information on interannual variability of the meridional overturning in the subpolar gyre region. Some time series of sea levels from the region extend back to before the start of the twentieth century (BH09). A process-based understanding of the variability inferred from sea level and surface flux data may promote the use of sea level observations for a century-long historical reconstruction, as well as future monitoring, of the subpolar overturning.

It might be expected that any change in the AMOC captured by the sea level signal would lag by a few years the signal in air–sea flux that caused the water mass transformation. That this is not evident in Fig. 8b may partially reflect the fact that the lag will depend on exactly where the NADW is formed from air–sea fluxes. A range of coupled climate models (Grist et al. 2009; Langehaug et al. 2012) and an ocean model (Grist et al. 2012) suggest that changes in the transformation rate of water into the NADW density range precedes changes in the AMOC by 3–5 years. Specifically, the model results of Grist et al. (2009, 2012) indicate that the best representation of the AMOC variability can be achieved by averaging the maximum transformation rate in the relevant θ–σ range over the previous 10 years. Using that approach, the 12 reanalysis-based estimates of the temporal evolution AMOC anomalies are shown in Fig. 8c.

The two six-member ensemble means associated with the different salinity products are shown in Fig. 8d. Also shown on Fig. 8d is the anomalous maximum strength of the AMOCσ at 45°N from a hindcast of the eddy-permitting ocean-only model, the Nucleus for European Modelling of the Ocean (NEMO) using a ¼° ORCA grid (ORCA025) (Madec 2008) (green line). The NEMO ORCA025 model provides realistic simulations of the large-scale temperature changes in the North Atlantic (Grist et al. 2010). As such, it is a useful tool for diagnosing the causes of circulation changes. The run depicted in Fig. 8d uses the NEMO version 3.2 code with 75 vertical levels and is forced with

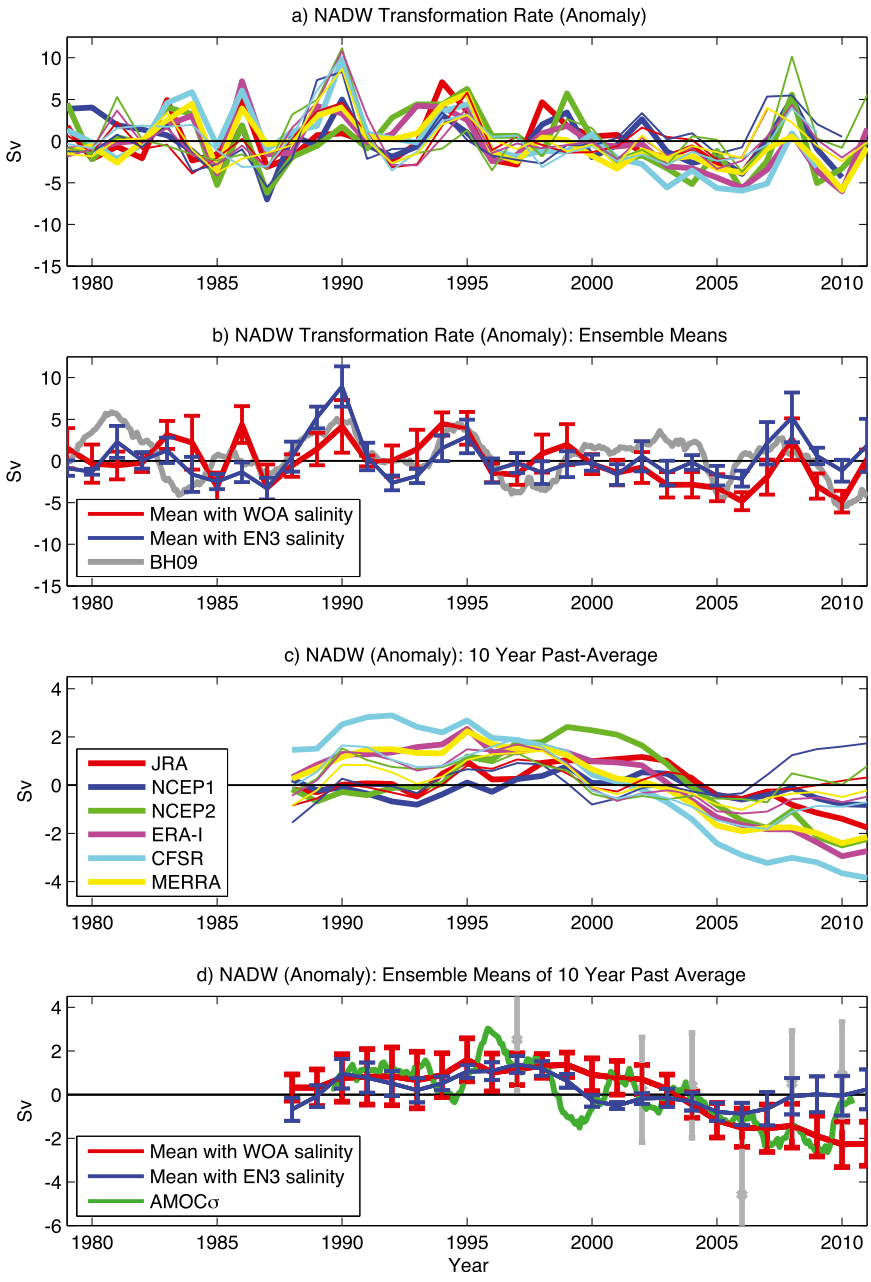

FIG. 8. (a) Time series of the annual maximum transformation rate (Sv) north of 45°N (NADW) from the surface-forced streamfunction. The thick lines indicate estimates calculated with *WOA* SSS and the thin lines indicate estimates calculated with EN3 SSS. The atmospheric reanalysis used for SST and the surface fluxes are indicated in the legend in (c). (b) Ensemble means of the *WOA* (red line) and EN3 (blue line) estimates in (a). The error bars indicate standard deviations of the six estimates. The gray line is the mean sea level anomaly (cm) of 10 stations between Yarmouth and New York (multiplied by −1) updated from BH09. As explained in the text, the sea level variability may be indicative of variations in AMOC strength. (c) The 10-yr past average of the NADW transformation rates in (a), where the same color key for (a) applies. (d) The 10-yr past average of the NADW transformation rates in (b) (red and blue lines). Anomalous maximum strength of AMOCσ at 45°N from the NEMO ORCA025 model hindcast (green line). Gray vertical bars denote AMOCσ estimates (with error range) from six Fourex/OVIDE occupations (Mercier et al. 2014), where departures from the six-occupation mean are plotted.

ERA-I surface meteorological fields. It has recently been used to investigate the 2009–10 30% reduction in AMOC strength (Blaker et al. 2014, manuscript submitted to *Climate Dyn.*). Although the model simulation inevitably shows a higher degree of interannual variability than the time-averaged surface estimates, there is some agreement in the lower-frequency variability. In particular, surface flux estimates and the hindcast provide some indication that there was an anomalously strong AMOCσ in the mid- to late 1990s and a decline in strength from 1999 to 2005. Since 2005 the surface flux based estimates of AMOCσ (45°N) have been either anomalously weak (using *WOA* salinity) or near normal (using EN3 salinity) depending on the salinity product used. We note the temporal evolution shown in Figs. 8c and 8d has a different character from other Walin surface-flux based descriptions of the overturning (Marsh 2000; Lumpkin et al. 2008), primarily due to our attempt to account for the lag between surface fluxes and AMOCσ.

While acknowledging the caveats previously mentioned in section 4a, as well as the additional question of the extent to which a month-long hydrographic section represents the annual mean, our results in Fig. 8d are also compared with AMOCσ estimates from six Fourex/OVIDE occupations between 1997 and 2010 (Mercier et al. 2014). When averaged together, the different surface-flux estimates suggest that the subpolar AMOCσ experienced a decrease (~2 Sv) between the late 1990s and 2006. The OVIDE measurements also indicate a change in the same sense during this period, although the magnitude of the decline is larger (~6 Sv). Although the OVIDE line is upstream of Labrador Seawater formation, there is additional evidence that changes in LSW formation rate during this period were in the same sense. First, biennial estimates of the LSW formation rates between 1997 and 2005 from chlorofluorocarbon (CFC) inventories (Rhein et al. 2011) indicate a steady decline over the period. Second, an analysis of five hydrographic sections at 48°N downstream of LSW formation (Lumpkin et al. 2008) suggests that the AMOC weakened between 1997 and 2000, although these changes are just within the error ranges. From 2006 to 2010, both the OVIDE measurements and the EN3-based estimates indicated that the subpolar AMOCσ was close to the long-term mean, whereas for the *WOA*-based estimate the AMOCσ remained weaker than the mean.

b. Subtropical circulation and STMW formation

In a similar manner to Marsh (2000), a time series of the subtropical transformation rate associated with air–sea fluxes is constructed from the maximum annual value of $F(\theta, \sigma)$ in the zone 20°–40°N and for $25.175 < \sigma < 26.375\,\mathrm{kg\,m^{-3}}$. The anomalies of these values for the 12 estimates are plotted as a time series in Fig. 9a. The temporal pattern of variability in subtropical transformation rate for 1979–2011 depicted by the ensemble means is dominated by the anomalous high rate in 1995–96 followed by an anomalously low rate in 1998. Prior to (after) this event, the average subtropical rate was slightly lower (higher) than for the whole period.

There is much greater disagreement between the subtropical estimates than is the case in the subpolar regions. In the subtropics correlation coefficients between the different estimates lie between −0.03 and 0.79, compared to 0.48–0.90 for NADW, with a mean of 0.47, compared to 0.71 for NADW. The standard deviation of each time series ranges between 3.6 and 6.6 Sv. Again, this is a larger range than for NADW. The implication is that estimates of subtropical variability are more sensitive to the choice of atmospheric reanalysis, as suggested for the mean values. Indeed, the choice of atmospheric reanalysis can lead to very different (i.e., uncorrelated) depictions of recent variability in the surface-forced subtropical circulation.

In Fig. 9b, we plot the mean of the six estimates with *WOA* salinity along with the mean of the six estimates with EN3 salinity. The error bars show the respective standard deviations. The two ensemble means are similar, falling within the error bars in all but two years (1996 and 2002). While this does not represent any verification of the salinity products or the method itself, it does at least imply that the uncertainty associated with choice of salinity product does not limit the utility of the Walin method to estimate the surface-forced STMW transformation rate.

The temporal evolution of the (anomalous) volume of STMW associated with the surface fluxes can be estimated from the time-varying surface-forced streamfunction. Using the relationship in Eq. (3) and the reanalysis-based estimates of $F(\theta, \sigma)$ for the western half of the basin, 12 time series of the STMW formation rates have been calculated. The time integral of the STMW formation rate yields the inferred change in its volume, where, following KR04, in order to account for STMW turnover time scale, the appropriate time scale for the time integration of $M(\sigma)$ is 4 years.

The calculated estimates of anomalous STMW volume were compared with observations of STMW volume change from subsurface temperature observations; an extended time series of KR04 is described in section 3d. The correlation coefficient between each atmospheric reanalysis-based estimate and the KR04 observational analysis is displayed in Fig. 10a. The level of correlation ranges from negligible or negative to $r = 0.65$ for JRA with *WOA* salinity. Two of the 12 flux-based estimates (JRA and NCEP2, both with *WOA*

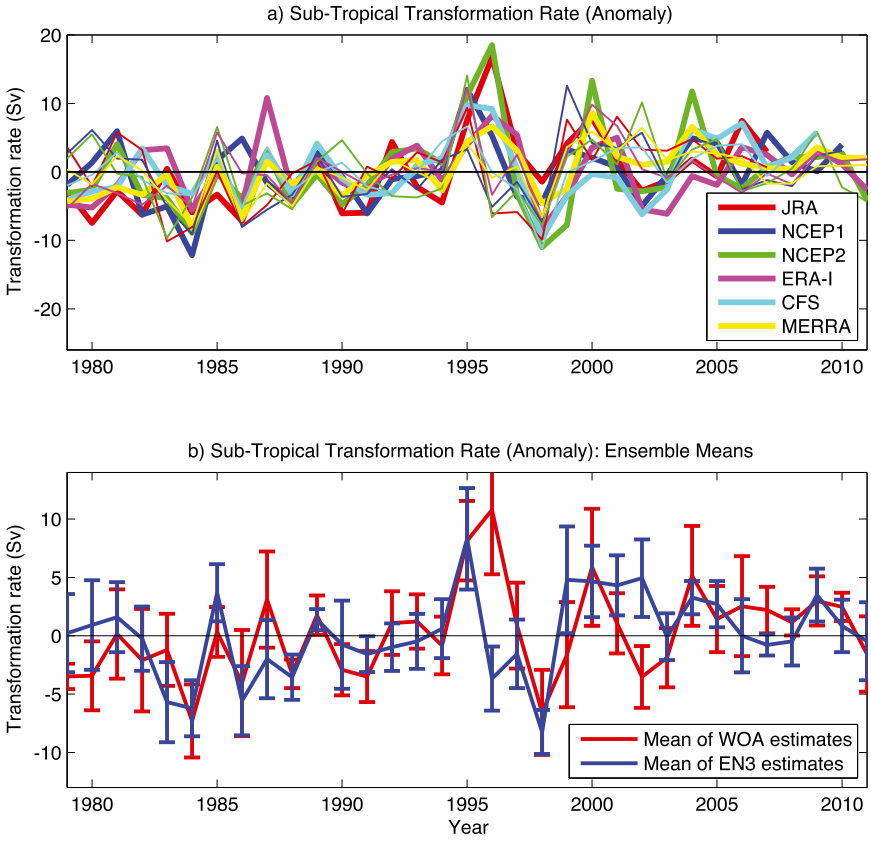

FIG. 9. (a) Time series of the annual maximum transformation rate (Sv) between 20° and 40°N and for $25.175 < \sigma < 26.375\,\mathrm{kg\,m^{-3}}$ (STMW) from the surface-forced streamfunction. Values are plotted as anomalies from the 1979–2007 mean. The thick lines indicate estimates calculated with *WOA* SSS and the thin lines indicate estimates calculated with EN3 SSS. The atmospheric reanalysis used in for SST and the surface fluxes are indicated in the legend. (b) Ensemble means of the *WOA* (red line) and EN3 (blue line) estimates in (a). The error bars indicate standard deviations of the six estimates.

salinity) of volume change have a statistically significant correlation at the 99% level (Bretherton et al. 1999). The feasibility of using the Walin approach for estimating temporal changes in STMW volume thus appears to be critically dependent on the choice of reanalysis product.

The extended time series of KR04 is plotted in Fig. 10c alongside the two flux-derived estimates that are significantly correlated with it. The flux-based estimates display a decreasing volume in the 1980s and early 1990s. Between the late 1990s and 2005, there is an increase in volume back to the 1980 level. Between 2005 and 2011, there is a small increase. As the magnitude of the temporal variability is greater with the surface flux–based estimates, the time series are normalized by their minimum value (Fig. 10d), to more clearly illustrate their level of agreement. As shown in Fig. 10b, for the flux estimates with the significant correlation, the standard deviation is 3.9 (for JRA) and 5.9 (for NCEP2) times the observed value. Thus, although using the Walin approach with two of the current reanalysis surface flux products yields STMW volume change estimates that are significantly correlated with subsurface observations, the amount of variance explained is relatively modest (i.e., up to 42% with $r = 0.65$), and the magnitudes of the volume changes appear to be markedly overestimated. It therefore appears that, even when using JRA and NCEP2 surface fluxes to apply the Walin approach in the subtropics, other processes effecting STMW volume change should be quantified. We note that diapycnal mixing, and seasonal mixed layer entrainment in particular, acts in opposition to surface-forced water mass transformation in the subtropics (Speer and Tziperman 1992; Nurser et al. 1999), suppressing the amplitude of STMW formation rates.

Summarizing this section, it has been shown that temporal variability of the subpolar transformation rate is broadly similar, regardless of the atmospheric reanalysis

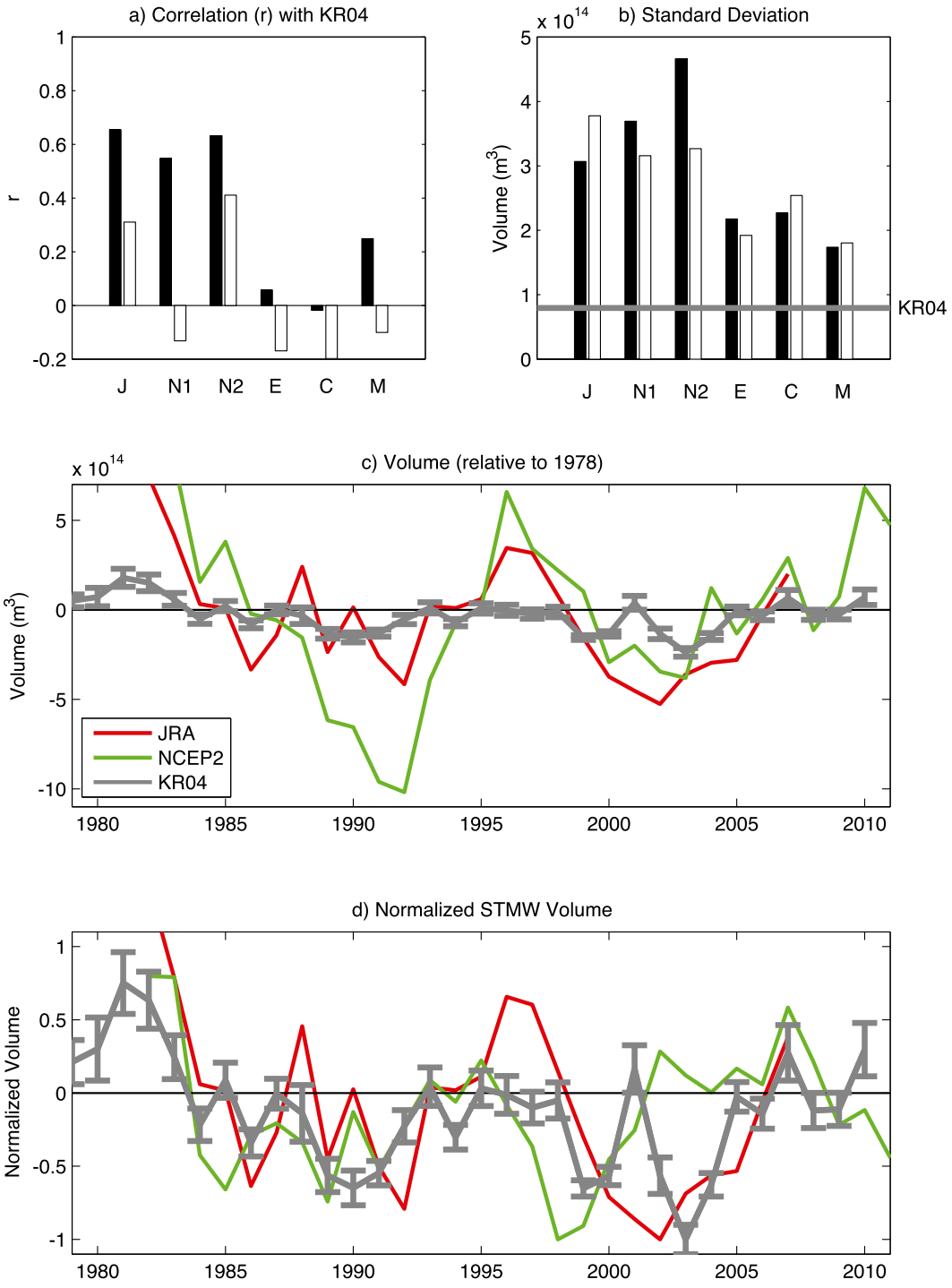

FIG. 10. (a) Correlation coefficient for the relationship between the 12 reanalysis-based estimates of anomalous STMW volume with the estimate from subsurface temperature observations (KR04). (b) Standard deviation of anomalous STMW volume time series. The standard deviation from the updated KR04 estimates is also indicated. In (a) and (b) the different reanalysis products are indicated as follows: J is JRA, N1 is NCEP1, N2 is NCEP2, E is ERA-I, C is CFSR, and M is MERRA. The black (white) bars denote estimates with *WOA* (EN3) SSS. (c) Time series of anomalous STMW volume (relative to 1978) from KR04 and the two reanalyses based estimates that are significantly correlated with KR04 (JRA; red line) and NCEP2 (green line) with *WOA* SSS. (d) As in (c), but time series have normalized by their minimum value.

or SSS product used. In itself, this finding provides no validation of accuracy in the reanalysis-derived surface density fluxes. However, it does suggest that the spread of uncertainty from these reanalyses is not so large as to invalidate their use to estimate the surface-forced overturning in subpolar latitudes. To this end, an estimate of the recent variability in the AMOCσ at 45°N based on the 10-yr past averaging of the NADW signal was presented. In contrast to the subpolar region, reanalysis-based estimates of the subtropical surface-forced circulation show relatively low levels of agreement. It is also clear that further consideration of the role of mixing processes is required to reconcile the magnitude of surface flux estimated volume changes with those from in situ observations.

6. Summary and conclusions

In this paper we have examined the range of depictions of the North Atlantic surface-forced streamfunction arising from a set of six modern-era atmospheric reanalyses. The surface-forced streamfunction is a potentially powerful tool for ongoing monitoring of the subpolar AMOCσ and may also provide insight into temporal variability in the volume of STMW (e.g., Grist et al. 2012; Marsh 2000). The primary motivation for the research presented here is to evaluate the extent to which inferring the mean and time-varying strength of the surface-forced overturning circulation is limited by uncertainty associated with the differences in these air–sea flux datasets.

The different reanalysis-based estimates of the surface-forced streamfunction all display a positive clockwise cell depicting the northward bound water becoming denser, sinking, and returning south at depth, consistent with ocean state estimates of AMOCσ. In the regions associated with NADW formation, it does not appear that the spread of estimates from different reanalysis products limits the feasibility of using the surface-forced overturning to estimate subpolar AMOCσ. Specifically, it was found that reanalysis-based estimates of the overturning strength ranged from 12 to 18 Sv. Although not an exactly comparable circulation measure, because of reasons mentioned in the text, it was noted that these estimates fall within the range of AMOCσ estimates from six hydrographic occupations of the Greenland (60°N) to Portugal (40°N) OVIDE line between 1997 and 2010 (Lherminier et al. 2007; 2010; Gourcuff et al. 2011; Mercier et al. 2014). In addition, the temporal variabilities of the different estimates are well correlated with one another; the correlation coefficient varies between 0.48 and 0.90 with a mean value of 0.71. The choice of salinity product does not appear to greatly affect either the mean state or the temporal variability.

It is important to note that a robust evaluation of the ability of state-of-the-art reanalysis-based surface-forced estimates to infer the temporal evolution of the AMOCσ would require a comparison against continuous independent measurement from this subpolar latitude. Although such measurements do not currently exist, using the surface-forced overturning estimates in conjunction with other physically based proxies may provide a way of increasing understanding of the subpolar overturning. As an example of this, we have attempted to connect our analysis results to the method of BH09, who invoke geostrophy to argue that the sea level along the eastern U.S. seaboard should be indicative of the strength of the overturning. There are some similarities between the time series of NADW transformation derived from reanalysis-based estimates of the surface-forced streamfunction and the BH09 signal. However, the two time series are not significantly correlated over the entire length of the study period. Further work, with ocean models as well as observations, will be required to elucidate the relationship between the two physical signals.

Earlier work has shown that the 10-yr past average of the surface-forced NADW signals explains a large part of the decadal variability in the subpolar AMOCσ. This result has been shown in relatively coarse-resolution climate models and an eddy-permitting ocean-only model (Josey et al. 2009; Grist et al. 2012). On this basis, we have presented calculations of the 10-yr past average of the surface-forced NADW transformation rate using surface flux fields from six atmospheric reanalyses. These measures of the anomalous subpolar AMOCσ strength suggest that in the mid-1990s the AMOCσ was anomalously strong, while between 1995 and 2005 the strength declined, and between 2005 and 2011 it has either been anomalously weak or near normal, depending on the salinity product used. The inferred temporal evolution is similar to the low-frequency component of AMOCσ in a hindcast of a ¼° eddy-resolving ocean-only model. Although this falls short of an observational validation of the method, the model used has been shown to simulate well the observed historical changes in the North Atlantic temperature (Grist et al. 2010). There is also supporting evidence from in situ observations that the subpolar overturning declined between the late 1990s and the middle of the following decade (Lumpkin et al. 2008; Rhein et al. 2011; Mercier et al. 2014). However, the main implication of our analysis is that because the subpolar reanalysis estimates are relatively similar, the uncertainty associated with the choice of product in itself does not critically limit their use for

this application. That is, they are potentially useful for inferring the evolution of subpolar AMOCσ from the surface-forced streamfunction.

In contrast to the subpolar latitudes, there is less agreement in the reanalysis-based estimates of the surface-forced streamfunction in the subtropics. The maximum mean transformation rate in the θ–σ space associated with STMW ranges from 6 to 30 Sv and some of the time series are uncorrelated. The large differences in the estimates at least partially reflect the difference in the thermal density flux (or net heat flux) across the breadth of the subtropical basin. For example, at 36°N JRA has heat loss across the whole width of the basin, whereas MERRA heat loss is restricted to the west of 50°W. The time-integrated estimates of surface-forced streamfunction were related to an independent estimate of STMW volume change (KR04). Despite the aforementioned uncertainty in the reanalyses time series, a subset of the estimates were significantly correlated with the independent estimate, capturing the decline in volume between 1980 and 1990 and the volume increase between 1995 and 2010. However, the magnitude of the surface flux estimated changes are 4–6 times that of the independent estimate. The inability of estimates from surface flux products to close the STMW volume budget has been noted elsewhere. It partially reflects the significant role of seasonal entrainment and lateral fluxes in damping the STMW formation rate. In addition, Forget et al. (2011) recently concluded that, even accounting for the effect of lateral fluxes, reanalysis products need a spatially nonuniform adjustment in order to be reconciled with observed volume changes. Thus, even though some of the modern-era reanalyses considered here correlate with observed STMW volume changes, this subset requires further evaluation (e.g., with observations from research buoys and ships) and/or physically based adjustment (e.g., consistency with ocean heat transport and global heat budget balance) in order for their depictions of the subtropical surfaced-forced overturning to be considered reliable.

In the tropical region, the MERRA, CFSR, and ERA-I reanalysis datasets depict counter circulation cells depicting equatorward-flowing surface water becoming lighter. These cells, which are up to 20 Sv and span from the equator to 40°N, are indicative of a high surface heat flux (oceanic gain) in the tropics and subtropics. This unrealistic feature appears to be a function of the bias in the global heat budget in the three datasets. The mean net global ocean heat gain is 11, 13, and 19 W m^{-2} in ERA-I, CFSR, and MERRA, respectively.

In summary, a set of six reanalysis products covering the modern era (1979–2011) has been used to estimate the surface-forced component of the North Atlantic meridional overturning circulation. In the region associated with NADW formation, the strength of the overturning is within the range of recent hydrographic estimates and time series from the different estimates are well correlated with one another. As such, uncertainty stemming from the spread of estimates based on the reanalyses does not in itself appear to limit the feasibility of inferring a surface-forced streamfunction in the subpolar region. Therefore the reanalyses (along with observed SSS fields) may potentially be used to estimate ongoing AMOCσ changes in the subpolar region, where there is currently no dedicated observing array. In contrast to the subpolar regions, the reanalyses yield a wide range of estimates in the inferred mean tropical and subtropical surface-forced circulation and their time series are poorly correlated with one another. A large part of the spread in the estimates of the mean surface-forced circulation of the subtropics is associated with biases in the global ocean heat budgets implied from the atmospheric reanalyses. Consequently, although a subset of the reanalyses are able to explain a significant amount of the variance in changes of STMW volume, it would be appropriate for considerable caution, further evaluation, and possible adjustment to accompany their future use for estimating the surface-forced overturning in the subtropics.

Acknowledgments. JPG is funded by UK Natural Environment Research Council New Investigator Grant NE/I001654/1. Y-OK was supported by the U.S. National Science Foundation under Grant OCE-0424492. RJB is supported by a fellowship from the UK National Centre for Earth Observation.

REFERENCES

Antonov, J. I., and Coauthors, 2010: *Salinity.* Vol. 2, *World Ocean Atlas 2009,* NOAA Atlas NESDIS 69, 184 pp.

Bingham, R. J., and C. W. Hughes, 2008: Determining North Atlantic meridional transport variability from pressure on the western boundary: A model investigation. *J. Geophys. Res.,* **113,** C09008, doi:10.1029/2007JC004679.

——, and ——, 2009: Signature of the Atlantic meridional overturning circulation in sea level along the east coast of North America. *Geophys. Res. Lett.,* **36,** L02603, doi:10.1029/2008GL036215.

——, ——, V. Roussenov, and R. G. Williams, 2007: Meridional coherence of the North Atlantic meridional overturning circulation. *Geophys. Res. Lett.,* **34,** L23606, doi:10.1029/2007GL031731.

Bretherton, C. S., M. Widmann, V. P. Dymnikov, J. M. Wallace, and I. Bladé, 1999: The effective number of spatial degrees of freedom in a time-varying field. *J. Climate,* **12,** 1990–2009, doi:10.1175/1520-0442(1999)012<1990:TENOSD>2.0.CO;2.

Cunningham, S. A., and Coauthors, 2007: Temporal variability of the Atlantic meridional overturning circulation at 26.5°N. *Science,* **317,** 935–938, doi:10.1126/science.1141304.

da Silva, A. M., C. C. Young, and S. Levitus, 1994: *Algorithms and Procedures.* Vol. 1, *Atlas of Surface Marine Data 1994,* NOAA Atlas NESDIS 1, 51 pp.

Davis, X. J., F. Straneo, Y.-O. Kwon, K. A. Kelly, and J. M. Toole, 2013: Evolution and formation of North Atlantic Eighteen Degree Water in the Sargasso Sea from moored data. *Deep-Sea Res. II,* **91,** 11–24, doi:10.1016/j.dsr2.2013.02.024.

Dee, D. P., and Coauthors, 2011: The ERA-Interim reanalysis: Configuration and performance of the data assimilation system. *Quart. J. Roy. Meteor. Soc.,* **137,** 553–597, doi:10.1002/qj.828.

Dickson, R. R., and J. Brown, 1994: The production of North Atlantic Deep Water: Sources, rates and pathways. *J. Geophys. Res.,* **99,** 12 319–12 341, doi:10.1029/94JC00530.

Fiorino, M., 2004: A multi-decadal daily sea surface temperature and sea ice concentration data set for the ERA-40 reanalysis. ERA-40 Rep. 12, ECMWF, 16 pp.

Forget, G., G. Maze, M. Buckley, and J. Marshall, 2011: Estimated seasonal cycle of North Atlantic Eighteen Degree Water volume. *J. Phys. Oceanogr.,* **41,** 269–286, doi:10.1175/2010JPO4257.1.

Getzlaff, J. C., C. W. Böning, C. Eden, and A. Biastoch, 2005: Signal propagation related to the North Atlantic overturning. *Geophys. Res. Lett.,* **32,** L09602, doi:10.1029/2004GL021002.

Gourcuff, C., P. Lherminier, H. Mercier, and P. Y. LeTraon, 2011: Altimetry combined with hydrography for ocean transport estimation. *J. Atmos. Oceanic Technol.,* **28,** 1324–1337, doi:10.1175/2011JTECHO818.1.

Grist, J. P., and S. A. Josey, 2003: Inverse analysis adjustment of the SOC air–sea flux climatology using ocean heat transport constraints. *J. Climate,* **16,** 3274–3295, doi:10.1175/1520-0442(2003)016<3274:IAAOTS>2.0.CO;2.

——, ——, and B. Sinha, 2007: Impact on the ocean of extreme Greenland Sea heat loss in the HadCM3 coupled ocean–atmosphere model. *J. Geophys. Res.,* **112,** C04014, doi:10.1029/2006JC003629.

——, R. Marsh, and S. A. Josey, 2009: On the relationship between the North Atlantic meridional overturning circulation and the surface-forced overturning stream function. *J. Climate,* **22,** 4989–5002, doi:10.1175/2009JCLI2574.1.

——, and Coauthors, 2010: The roles of surface heat flux and ocean heat transport convergence in determining Atlantic Ocean temperature variability. *Ocean Dyn.,* **60,** 771–790, doi:10.1007/s10236-010-0292-4.

——, S. A. Josey, and R. Marsh, 2012: Surface estimates of the Atlantic overturning in density space in an eddy-permitting model. *J. Geophys. Res.,* **117,** C06012, doi:10.1029/2011JC007752.

Hakkinen, S., P. B. Rhines, and D. Worthen, 2011: Warm and saline events embedded in the meridional circulation of the northern North Atlantic. *J. Geophys. Res.,* **116,** C03006, doi:10.1029/2010JC006275.

Hansen, B., and S. Østerhus, 2000: North Atlantic–Nordic Seas exchanges. *Progr. Oceanogr.,* **45,** 109–208, doi:10.1016/S0079-6611(99)00052-X.

——, and ——, 2007: Faroe Bank Channel overflow 1995–2005. *Prog. Oceanogr.,* **75,** 817–856, doi:10.1016/j.pocean.2007.09.004.

Hobbs, W. R., and J. K. Willis, 2012: Midlatitude North Atlantic heat transport: A time series based on satellite and drifter data. *J. Geophys. Res.,* **117,** C01008, doi:10.1029/2011JC007039.

Howe, N., and A. Czaja, 2009: A new climatology of air–sea density fluxes and surface water mass transformation rates constrained by WOCE. *J. Phys. Oceanogr.,* **39,** 1432–1447, doi:10.1175/2008JPO4025.1.

Ingleby, B., and M. Huddleston, 2007: Quality control of ocean temperature and salinity profiles—Historical and real-time data. *J. Mar. Syst.,* **65,** 158–175, doi:10.1016/j.jmarsys.2005.11.019.

Isemer, H.-J., and L. Hasse, 1987: *Air–Sea Interactions.* Vol. 2, *The Bunker Climate Atlas of the North Atlantic Ocean,* Springer-Verlag, 218 pp.

Ishii, M., A. Shouji, S. Sugimoto, and T. Matsumoto, 2005: Objective analyses of sea-surface temperature and marine meteorological variables for the 20th century using ICOADS and the KOBE collection. *Int. J. Climatol.,* **25,** 865–879, doi:10.1002/joc.1169.

Johns, W. E., and Coauthors, 2011: Continuous, array-based estimates of Atlantic Ocean heat transport at 26.5°N. *J. Climate,* **24,** 2429–2449, doi:10.1175/2010JCLI3997.1.

Johnson, H. L., and D. P. Marshall, 2002: A theory for the surface Atlantic response to thermohaline variability. *J. Phys. Oceanogr.,* **32,** 1121–1132, doi:10.1175/1520-0485(2002)032<1121:ATFTSA>2.0.CO;2.

Josey, S. A., J. P. Grist, and R. Marsh, 2009: Estimates of meridional overturning circulation variability in the North Atlantic from surface density flux fields. *J. Geophys. Res.,* **114,** C09022, doi:10.1029/2008JC005230.

Joyce, T. M., 2012: New perspectives on Eighteen-Degree Water formation in the North Atlantic. *J. Oceanogr.,* **68,** 45–52, doi:10.1007/s10872-011-0029-0.

Kalnay, E., and Coauthors, 1996: The NCEP/NCAR reanalysis project. *Bull. Amer. Meteor. Soc.,* **77,** 437–471, doi:10.1175/1520-0477(1996)077<0437:TNYRP>2.0.CO;2.

Kanamitsu, M., W. Ebisuzaki, J. Woollen, S.-K. Yang, J. J. Hnilo, M. Fiorino, and G. L. Potter, 2002: NCEP-DEO AMIP-II Reanalysis (R-2). *Bull. Amer. Meteor. Soc.,* **83,** 1631–1643, doi:10.1175/BAMS-83-11-1631.

Kanzow, T., and Coauthors, 2007: Observed flow compensation associated with the MOC at 26.5°N in the Atlantic. *Science,* **317,** 938–941, doi:10.1126/science.1141293.

——, and Coauthors, 2010: Seasonal variability of the Atlantic meridional overturning circulation at 26.5°N. *J. Climate,* **23,** 5678–5698, doi:10.1175/2010JCLI3389.1.

Kwon, Y.-O., 2003: Observation of general circulation and water mass variability in the North Atlantic subtropical mode water region. Ph.D. thesis, University of Washington, 161 pp.

——, and S. C. Riser, 2004: North Atlantic Subtropical Mode Water: A history of ocean–atmosphere interaction 1961–2000. *Geophys. Res. Lett.,* **31,** L19307, doi:10.1029/2004GL021116.

Langehaug, H. R., P. B. Rhines, T. Eldevik, K. Lohmann, and J. Mignot, 2012: Water mass transformation and the North Atlantic Current in three multi-century climate model simulations. *J. Geophys. Res.,* **117,** C11001, doi:10.1029/2012JC008021.

Lherminier, P., H. Mercier, C. Gourcuff, M. Alvarez, S. Bacon, and C. Kermabon, 2007: Transports across the 2002 Greenland-Portugal Ovide section and comparison with 1997. *J. Geophys. Res.,* **112,** C07003, doi:10.1029/2006JC003716.

——, ——, T. Huck, C. Gourcuff, F. F. Perez, P. Morin, A. Sarafanov, and A. Falina, 2010: The Atlantic meridional overturning circulation and the subpolar gyre observed at the A25-OVIDE section in June 2002 and 2004. *Deep-Sea Res. I,* **57,** 1374–1391, doi:10.1016/j.dsr.2010.07.009.

Lumpkin, R., and K. G. Speer, 2003: Large-scale vertical and horizontal circulation in the North Atlantic Ocean. *J. Phys. Oceanogr.,* **33,** 1902–1920, doi:10.1175/1520-0485(2003)033<1902:LVAHCI>2.0.CO;2.

——, ——, and K. P. Koltermann, 2008: Transport across 48°N in the Atlantic Ocean. *J. Phys. Oceanogr.,* **38,** 733–752, doi:10.1175/2007JPO3636.1.

Macrander, A., U. Send, H. Valdimarsson, S. Jónsson, and R. H. Käse, 2005: Interannual changes in the overflow from the Nordic seas into the Atlantic Ocean through Denmark Strait. *Geophys. Res. Lett.,* **32,** L06606, doi:10.1029/2004GL021463.

Madec, G., 2008: NEMO ocean engine. Note du Pole de modelisation 27, IPSL, 209 pp.

Marsh, R., 2000: Recent variability of the North Atlantic thermohaline circulation inferred from surface heat and freshwater fluxes. *J. Climate,* **13,** 3239–3260, doi:10.1175/1520-0442(2000)013<3239:RVOTNA>2.0.CO;2.

McCarthy, G. D., and Coauthors, 2012: Observed interannual variability of the Atlantic meridional overturning circulation at 26.5°N. *Geophys. Res. Lett.,* **39,** L19609, doi:10.1029/2012GL052933.

Mercier, H., and Coauthors, 2014: Variability of the meridional overturning circulation at the Greenland-Portugal OVIDE section from 1993 to 2010. *Prog. Oceanogr.,* doi:10.1016/j.pocean.2013.11.001, in press.

Nurser, A. J. G., R. Marsh, and R. G. Williams, 1999: Diagnosing water mass formation from air–sea fluxes and surface mixing. *J. Phys. Oceanogr.,* **29,** 1468–1487, doi:10.1175/1520-0485(1999)029<1468:DWMFFA>2.0.CO;2.

Onogi, K., and Coauthors, 2007: The JRA-25 Reanalysis. *J. Meteor. Soc. Japan,* **85,** 369–432, doi:10.2151/jmsj.85.369.

Reynolds, R. W., and T. M. Smith, 1994: Improved global sea surface temperature analyses using optimum interpolation. *J. Climate,* **7,** 929–948, doi:10.1175/1520-0442(1994)007<0929:IGSSTA>2.0.CO;2.

——, N. A. Rayner, T. M. Smith, D. C. Stokes, and W. Wang, 2002: An improved in situ and satellite SST analysis for climate. *J. Climate,* **15,** 1609–1625, doi:10.1175/1520-0442(2002)015<1609:AIISAS>2.0.CO;2.

Rhein, M., and Coauthors, 2011: Deep water formation, the subpolar gyre, and the meridional overturning circulation in the subpolar North Atlantic. *Deep-Sea Res. II,* **58,** 1819–1832, doi:10.1016/j.dsr2.2010.10.061.

Rienecker, M. M., and Coauthors, 2011: MERRA: NASA's Modern-Era Retrospective Analysis for Research and Applications. *J. Climate,* **24,** 3624–3648, doi:10.1175/JCLI-D-11-00015.1.

Saha, S., and Coauthors, 2010: The NCEP Climate Forecast System Reanalysis. *Bull. Amer. Meteor. Soc.,* **91,** 1015–1057, doi:10.1175/2010BAMS3001.1.

Schmitt, F. W., P. S. Bogden, and C. E. Dorman, 1989: Evaporation minus precipitation and density fluxes for the North Atlantic. *J. Phys. Oceanogr.,* **19,** 1208–1221, doi:10.1175/1520-0485(1989)019<1208:EMPADF>2.0.CO;2.

Speer, K., and E. Tziperman, 1992: Rates of water mass formation in the North Atlantic Ocean. *J. Phys. Oceanogr.,* **22,** 93–104, doi:10.1175/1520-0485(1992)022<0093:ROWMFI>2.0.CO;2.

Taylor, K. E., D. Williamson, and F. Zwiers, 2000: The sea surface temperature and sea-ice concentration boundary conditions for AMIP II simulations. PCMDI Rep. 60, Lawrence Livermore National Laboratory, 25 pp.

Walin, G., 1982: On the relation between sea-surface heat flow and thermal circulation in the ocean. *Tellus,* **34,** 187–195, doi:10.1111/j.2153-3490.1982.tb01806.x.

Woodworth, P. L., and R. Player, 2003: The permanent service for mean sea level: An update to the 21st century. *J. Coastal Res.,* **19,** 287–295. [Available online at http://www.jstor.org/stable/4299170.]

Zhang, R., 2010: Latitudinal dependence of Atlantic meridional overturning circulation (AMOC) variations. *Geophys. Res. Lett.,* **37,** L16703, doi:10.1029/2010GL044474.